IEEE Access
Multidisciplinary | Rapid Review | Open Access Journal

Received 20 April 2023, accepted 10 May 2023, date of publication 19 May 2023, date of current version 30 May 2023.

Digital Object Identifier 10.1109/ACCESS.2023.3277968

RESEARCH ARTICLE

Fault Ride Through and Intermittency Improvement of Renewable Energy Integrated MMC-HVDC System Employing Flywheel Energy Storage

MD ISMAIL HOSSAIN[1], WALEED M. HAMANAH[1], MD SHAFIUL ALAM[2], MD SHAFIULLAH[1], (Senior Member, IEEE), AND MOHAMMAD A. ABIDO[1,3,4], (Senior Member, IEEE)

[1]Interdisciplinary Research Center in Renewable Energy and Power Systems (IRC-REPS), King Fahd University of Petroleum and Minerals, Dhahran 31261, Saudi Arabia
[2]Applied Research Center for Environment and Marine Studies, King Fahd University of Petroleum and Minerals, Dhahran 31261, Saudi Arabia
[3]K. A. CARE Energy Research and Innovation Center, Dhahran 31261, Saudi Arabia
[4]Electrical Engineering Department, King Fahd University of Petroleum and Minerals, Dhahran 31261, Saudi Arabia

Corresponding author: Mohammad A. Abido (mabido@kfupm.edu.sa)

This work was supported in part by the Interdisciplinary Research Center for Renewable Energy and Power Systems (IRC-REPS), King Fahd University of Petroleum & Minerals (KFUPM), Saudi Arabia, under Project INRE2314; and in part by the K. A. CARE Energy Research and Innovation Center (ERIC), KFUPM.

ABSTRACT Modular multilevel converter (MMC)-based high voltage direct current (HVDC) transmission networks integrate remotely located distributed renewable energy resources (RER). The intermittent nature of RER and symmetrical and asymmetrical AC-side low-voltage faults produce operational difficulties. It reduces the MMC's ability to transfer the rated power, which raises the voltage of the HVDC link. Therefore, the MMC-HVDC network's fault ride-through (FRT) capabilities and the power fluctuation brought on by RER intermittency are potential challenges to the efficient integration of renewable energy resources. In response, this article suggests an energy control scheme for the flywheel energy storage of the PV-wind-MMC-HVDC system in order to regulate the HVDC-link voltage during low voltage faults at the point of common coupling (PCC) of the AC grids and to address the problem of power fluctuation caused by intermittent RER and sudden load changes. The suggested method eliminates the dynamic braking resistor (DBR) from the HVDC link and seamlessly integrates the RER without actively reducing renewable energy power during low voltage faults. To test the effectiveness of the proposed control method for the flywheel energy storage in reducing excess energy in the HVDC link, symmetrical and asymmetrical low voltage faults have been conducted. In addition, changes in wind speed, solar radiation, and temperature have been made to validate the flywheel energy management system's performance. A real-time digital simulator (RTDS) and dSPACE-based controller hardware in loop (CHIL) configuration with a complete system have been used to simulate and evaluate the entire system.

INDEX TERMS Modular multilevel converter, PV-wind integration, flywheel energy management system, AC side low voltage faults.

I. INTRODUCTION

The MMC for VSC-HVDC connection has been identified as one of the most promising technologies for integrating the RER because of its scalability, modularity, and compact footprint [1], [2], [3]. The AC grid can receive stability support from the MMC-HVDC connected RER, including the frequency regulation [4] and the dynamic voltage control [5]. However, the FRT capabilities of the MMC-HVDC network continue to be a significant obstacle. When a grid

The associate editor coordinating the review of this manuscript and approving it for publication was Xiaofeng Yang.

fault occurs, the onshore MMC's active power is abruptly reduced, making it impossible for wind farms to transmit their generated power entirely to the grid. Due to the power imbalance, the DC-link voltage increases quickly as the relevant capacitors get charged. The installation of dynamic braking resistors (DBR) and quick power reduction of wind farms (WF) are some current practices to prevent overvoltage in the HVDC link. The fault effects are minimized by dissipating the excess power from the HVDC link through the DBR [6], [7], [8], [9], [10], [11]. The benefit of these techniques is that grid faults do not impact WFs, but they require additional hardware, including breakers, braking resistors, and series parallel power electronics switches. Usually, DC choppers (in parallel connected dynamic braking resistors) are good for dissipating excess energy in the HVDC link during low voltage disturbances at the point of common coupling with the AC grid. However, it is unable to make up for any energy shortages brought on by intermittent renewable energy.

Rapid active power reduction can also be accomplished through the utilization of communication-based de-loading control [12], voltage droop control [13], [14], [15], [16], [17], [18], [19], [20], [21], [22], [23], [24], [25], [26], [27], and frequency modulation [28], [29], [30]. The DC-link communication channels with wind turbines (WT) eliminate the need for additional offshore converter control, but they also cause reliability and latency issues. As an alternative, the offshore grid frequency is raised in proportion to the DC voltage variation to perform the frequency modulation control. Unfortunately, the delayed active power response of the WF due to its poor df/dt tolerance severely restricts this technique. The voltage droop management enables a quick reduction in WF active power to simplify the FRT of coupled offshore MMC-HVDC-connected wind farms. A real power current reduction control is proposed for WTs to contribute to the fault ride-through requirements of the HVDC network, along with a small voltage droop control solution in [13], [14], [20], [21], [22], and [23]. However, this could lead to significant DC overvoltage because of the voltage signal processing delay in the filter and bandwidth constraints in the current signal management of WTs. To keep the DC voltage at the required level, the offshore converter quickly reduces the offshore grid voltage to zero in [15], [16], [17], [18], [19], [24], [25], [26], and [27]. The phase lock loop (PLL)-based wind turbine converters may experience synchronization problems using this technology, which does not require any changes to the WT control [31], [32], [33]. Two-stage droop control is proposed to enhance FRT and post-fault recovery for MMC-HVDC-connected offshore wind farms [34]. However, a simplified current source is used to represent the wind turbine, which ignores the turbine inertia that introduces delay for the rapid power reduction. Similarly, active power reduction-based DC-link overvoltage control also encounters delays due to the large inertia of the wind turbine, which prevents rapid changes in active power. In addition to the mentioned control strategy, the RER is highly intermittent and challenging to match users' demands. Within this context, energy storage systems (ESS) have been recognized as a key technology to address such intermittency and facilitate effective penetration of the RER into the electricity grids. The demand for light and high-capacity energy storage is rising in many different applications. One such application is large-scale ESS with different types of renewable generation. To mitigate or smooth out the fast transients due to uncontrollable circumstance changes such as solar radiation, temperature, and wind speed change, more energy storage systems are now deployed along with those renewable generation stations, raising the acceptability of such ways of electricity generation by utility companies. The battery energy storage system (BESS) has a high energy density, high cycle efficiency, and can maintain a charge for a prolonged period [35]. As a result, several utilities are turning to BESS for power leveling, voltage, and frequency management [36], [37], [38]. Due to its lightweight and high energy density, the lithium-ion battery is taking on a large portion of the actual storage device's role in grid applications [39], [40], [41], [42]. MMC-HVDC with battery energy storage systems has been studied to mitigate wind energy fluctuations [43], [44], [45], [46], [47], [48], [49], [50], [51], [52], [53]. However, transient faults have not been addressed. In addition, an average model for the converter and a simplified current source for the wind energy have been used for the analysis and results. In contrast, the high-power density supercapacitor is a short-duration power source with a fast dynamic response [54], [55], [56], [57], [58]. Through the assistance of the voltage source converter (VSC)-based HVDC-link during an AC-side fault, it offers a similar potential for fault riding capability [59], [60]. Besides self-discharging losses, supercapacitors are still expensive compared to batteries and flywheel energy storage.

The main issue with battery energy storage is limited power density, which requires large batteries to absorb the excess energy accumulated in the HVDC link during AC-side low voltage faults. Although the number of faults in the system is limited to a few per year, load changes that cause frequency shifts and changes in renewable energy sources are frequent, which requires energy storage with a large number of charge and discharge cycles. Therefore, the lifetime of a battery degrades due to frequent charging and discharging to support intermittent renewable energy and load changes [61]. A flywheel energy storage device can rapidly change ample power that can be utilized to control the additional energy during a low voltage disturbance [54], [61], [62]. In a flywheel ESS-based FRT support, excess energy is collected as kinetic energy depending on the rotating speed and mass [38], [57], [60], [63], [64], [65], [66], [67], [68]. Although the flywheel has a high self-discharging loss compared to a battery, it has almost no limit on charging and discharging cycles.

Flywheel energy storage was connected with an HVDC link through a separate MMC to mitigate wind energy

fluctuation [65]. Flywheel energy storage was used to store energy from the DC link during AC-side low-voltage disturbances. In addition, a small-scale prototype is developed to verify the proposed control scheme's efficacy. In contrast, non-real-time simulation software employed an average model to obtain the result. It considered only three-phase balanced faults, whereas unbalanced faults have not been considered. In addition, sudden load changes on the AC side have not been considered. Besides, the power rating of the MMC-HVDC system has not been mentioned, and a single high-power machine model was used to absorb excess energy during the AC side low voltage faults. Usually, induction motors with hundreds of MW of capacity are practically not available for the flywheel application. The DC link voltage regulation is within 1% due to AC side faults. However, less severe low-voltage faults on the AC side may cause a slight increase in the voltage of the DC link, which can divert power from AC-side injection to Flywheel energy storage. Similarly, a dual three-phase induction machine-based flywheel energy storage system was discussed for fault ride improvement MMC-HVDC system [69]. However, grid voltage and fault type were not shown in the results. In addition, a low-voltage (6 kV) MMC-HVDC system was considered for the simulation. The work [70] proposed a control scheme for the DFIG to absorb the excess energy in the DC link by increasing the rotor speed of the DFIG. However, it is required for the oversize machine to operate in high-speed mode during the low voltage disturbance, which is above the nominal speed. The control of a permanent magnet synchronous generator is relatively easier than that of an induction generator or doubly fed induction generator. Besides flywheel-based energy storage, the rotor's kinetic energy from a permanent magnet synchronous generator can be utilized for grid frequency support [71].

The research in this work presents a permanent magnet synchronous motor (PMSM)-based flywheel energy storage control strategy to manage the excess power in the HVDC link during AC-side low voltage faults in view of the points and problems highlighted above. To deal with the intermittent nature of the RER and abrupt load variation, it proposes a combined control approach based on shortages and actual power requirements. In summary, the key contributions compared to the work [65] are as follows:

- Comprehensive energy control approach for permanent magnet synchronous motor-based flywheel energy storage: (a) to regulate the HVDC-link voltage during the low voltage faults at the PCC of AC grids; (b) to address intermittency caused by the renewable energy generation fluctuation; and (c) to absorb excess energy during sudden load changes.
- Grid voltage is added in the control loop to separate the fault during low-voltage disturbances from normal operating voltage.
- Simulation and testing of the complete systems in the real-time digital simulator (RTDS) and dSPACE-based controller hardware in the loop (CHIL) with detailed converter models.

The remainder of the work is organized as follows: A brief description of the MMC-HVDC system and solar and wind energy is provided in Section II. Additionally, Section II illustrates the suggested control technique for the flywheel energy management system to regulate the excess power in the HVDC link and smooth out the transient brought on by the variation in solar and wind energy as well as the fast change in load. Section III presents thorough simulation findings for the augmentation of transient performance due to RER and load variation, as well as the management of the HVDC-link voltage during low-voltage AC-side transient faults. Section IV concludes by offering recommendations for future study directions.

II. MODELING AND CONTROLLER DESIGN

The system comprises PV and wind farms with a PMSM-based flywheel energy storage system, as depicted in Fig. 1. The MMC1 manages the HVDC-link voltage, whereas the MMC2 connects the AC grid with the PV-wind system. Similarly, MMC3 forms the AC grid for the PMSM-flywheel energy storage integration. Scaling the output from one unit of renewable energy and energy storage through a controlled current source and multiplier increases the system's capacity.

A. SOLAR AND WIND ENERGY GRID INTEGRATION THROUGH MMC2 AND MMC1

The main objective of converter control for solar and wind energy is the integration with the AC grid that MMC2 forms. Based on the power versus voltage (P-V) characteristics curve, it is known that the photovoltaic panel's maximum output power varies with solar radiation and temperature variation. In order to maximize power output from the PV system under any operational conditions (temperature and solar irradiation), the PV side converter's controller modifies the DC-link voltage employing the modified incremental conductance method. More information on how solar energy is integrated into the grid can be found in [9], [72], [73], and [74]. Similarly, the maximum power of wind energy varies with wind speed. Field-oriented control is used to follow the reference electromagnetic torque set by the optimal point of wind energy. The detailed design for the DFIG based wind energy grid integration can be found in [9], and [75]. MMC2 connects the AC grid with the PV-wind system, whereas MMC1 controls the HVDC-link voltage. The detailed design can be found in [76], [77], and [78].

B. PMSM BASED FLYWHEEL CONTROL

MMC1 regulates the HVDC link voltage, and MMC3 creates the AC voltage for the PMSM based flywheel integration. The grid side converter (GSC) operates in power control mode, which receives the reference power command due to low voltage disturbances at PCC1 or load variation or renewable energy variation. By controlling electromagnetic

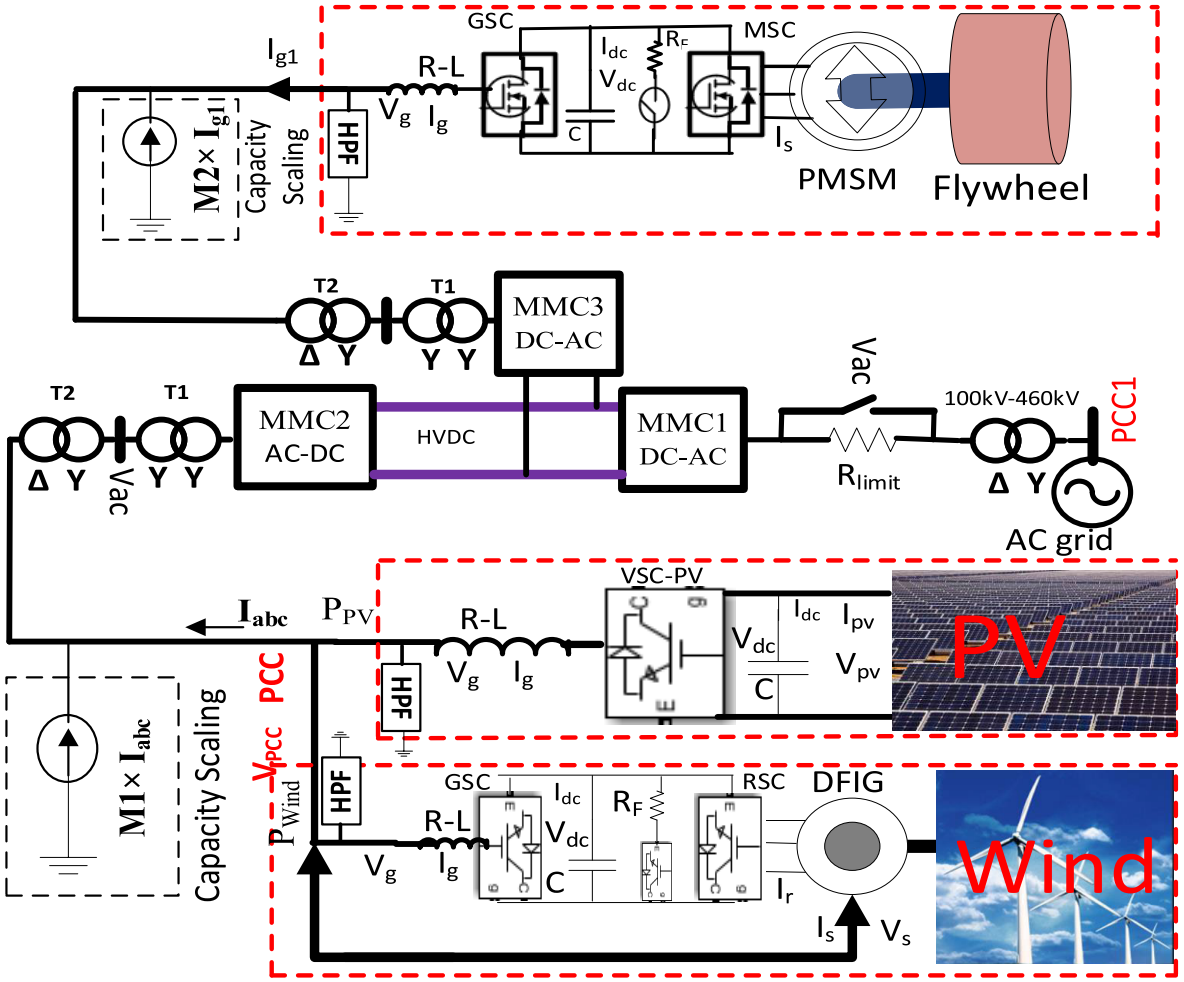

FIGURE 1. MMC-HVDC system with energy storage and renewable energy resources.

torque employing field-oriented control (FOC), PMSM can be worked as generator or motor.

During motoring operation, flywheel stores energy by increasing the rotor/flywheel speed, whereas it releases energy by decreasing the rotor/flywheel speed during generator operation. In rotor-field dq coordinate, the following equation dictates the PMSM stator current [75].

$$\left(\mathrm{L_d}\frac{di_d}{dt}+R_s i_d\right)=\mathrm{L_q}\omega i_q+V_d \tag{1}$$

$$\left(\mathrm{L_q}\frac{di_q}{dt}+R_s i_q\right)=-\mathrm{L_d}\omega i_d-\lambda_\mathrm{m}\omega+V_q \tag{2}$$

Unlike doubly fed induction motor and squirrel cage induction motor, only encoder retrieves the rotor flux position of PMSM. No external reactive power is required to operate PMSM.

Hence, reactive current of MSC is regulated at zero. Stator phase current is transformed into *dq* current with angle of rotor flux position.

$$\text{The electromagnetic torque,}\quad T_e=\frac{3}{2}\lambda_\mathrm{m}Pi_q \tag{3}$$

Equation (3) indicates that the q-axis current controls the electrical torque, while the reactive current remains zero. The q-axis current is generated from the DC link voltage regulation loop, which indirectly controls the electromagnetic torque as well as speed of flywheel. Finally, MSC current controller is formed based on equation (1) and equation (2). Fig. 2 (d) shows the PMSM side converter control. Any current deviation is processed through a PI controller ($\mathrm{PI_1}$), which is further added with the decoupling term and produces *dq* axis voltage for the MSC. Finally, the modulating signal (*abc*signal) is generated from the *dq* axis voltage with the help of rotor flux angle. The flywheel and PMSM rotor are connected via an axle. Hence, the rotor speed of PMSM is the flywheel speed.

C. PROPOSED ENERGY MANAGEMENT SYSTEM

The low voltage fault at the PCC1 of the MMC1, limits MMC1's power transfer capability, which raises the HVDC-link voltage. Usually, the dynamic braking resistor is placed in parallel with the transmission line for dissipation of the surplus energy to regulate the HVDC-link voltage within limits. To dissipate a significant quantity of the HVDC

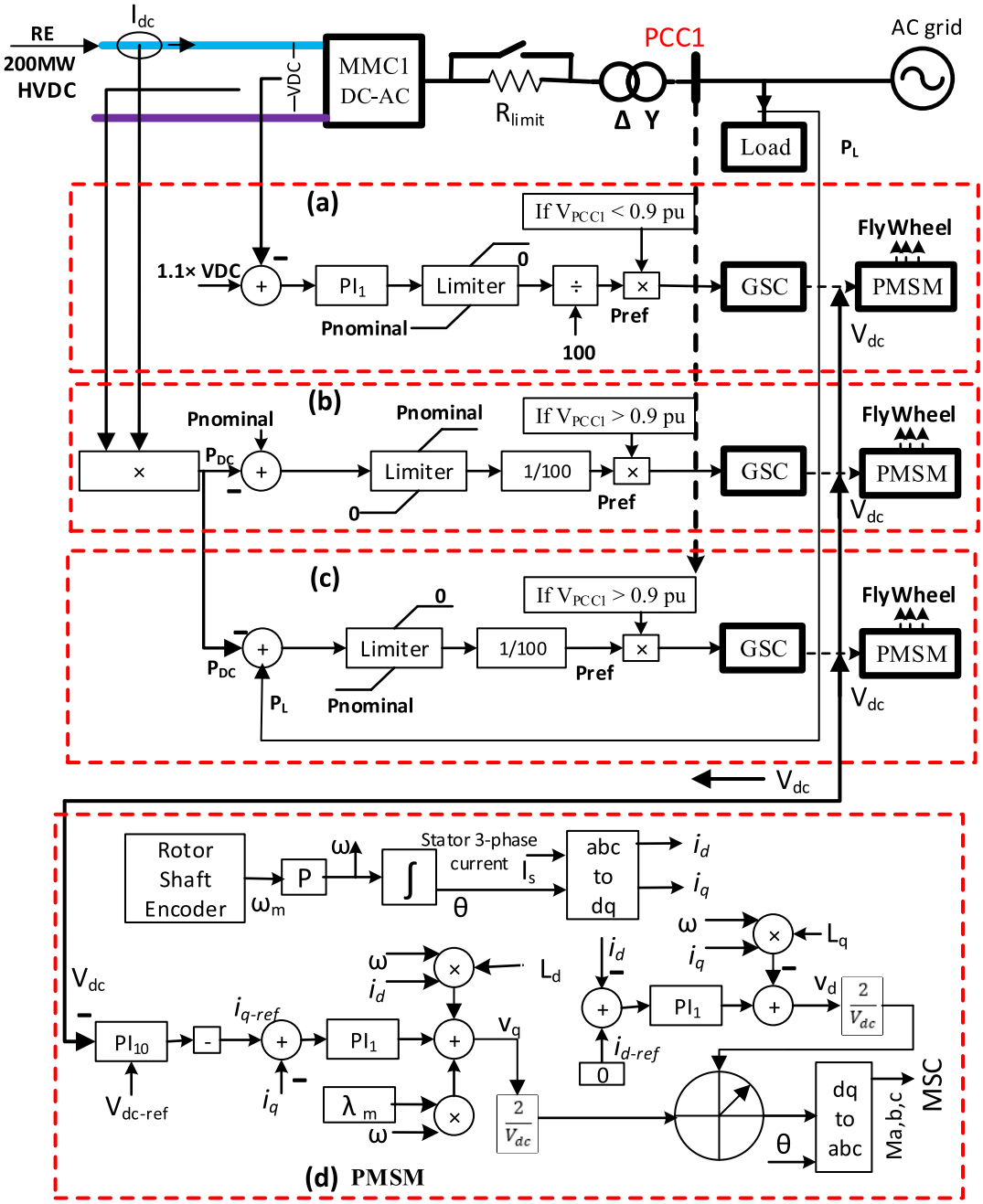

FIGURE 2. Control strategy of flywheel (a) HVDC-link's surplus energy control strategy (b) power leveling control strategy during the change in weather condition (wind speed, solar radiation, and temperature) (c) Excess power control during load disturbance, (d) Machine side converter control of PMSM.

power during the three-line-to-ground (LLLG) fault at the PCC of the AC grids, several series-parallel combination semiconductor switches are needed.

The HVDC connection voltage is subject to multiple switching introduced by the dynamic braking resistor, which may cause variations in the real power flow. Solar and wind energy are highly intermittent and change with the solar radiation, temperature, and wind speed change. Therefore, flywheel-based energy storage has been considered to address the renewable energy intermittency, smooth out the fast transients caused by the low voltage disturbances on the AC side and to absorb excess energy during sudden load change on the AC side. Besides, a flywheel is utilized to remove the DBR from the system.

1) AC SIDE LOW VOLTAGE FAULTS AT PCC1

During the low voltage faults at PCC1, the HVDC link voltage rises due to the capacity reduction of MMC1. Hence, the excess energy in the HVDC link is required to be delivered to the flywheel. When the HVDC link voltage goes above

1.1pu and the PCC voltage is below 0.9pu, the error is processed through the controller (PI_1) that produces the reference power command to the grid side converter (GSC), as shown in Fig. 2(a). The GSC operates in constant power control mode. The power injection by the GSC into the DC link raises the DC link voltage. The DC link voltage regulators (PI controller) as shown in Fig. 2(d) processes the DC link voltage deviation that generates the reference quadrature axis current (I_{q-ref}) or electromagnetic torque controlling current for the PMSM coupled flywheel. Finally, the speed of the flywheel is increased, which stores the excess energy from HVDC link. Thus, HVDC link voltage remains within the threshold.

2) INTERMITTENT RENEWABLE ENERGY

During normal grid voltage, the renewable energy intermittency is improved through the control action as shown in Fig. 2(b) The nominal power of renewable energy ($P_{nominal}$) is the combined PV and wind energy injected into the MMC1. Any deviation from the nominal power is compensated by the flywheel energy storage. As can be seen from Fig. 2(b), the difference between the nominal power of renewable energy and actual HVDC link power (P_{DC}) is used as the reference power command for the GSC. However, this time GSC transfers power from flywheel energy storage to HVDC link through the MMC3. Hence, DC link voltage of GSC is reduced. Again, the DC link voltage regulators (PI controller) as shown in Fig. 2(d) processes the DC link voltage deviation that generates the reference quadrature axis current (I_{q-ref}) or electromagnetic torque controlling current for the PMSM coupled flywheel. Finally, the speed of flywheel is decreased by releasing required shortage energy. Thus, the power injected by the MMC remains the same under renewable energy intermittent caused by the weather condition (wind speed, solar radiation, and temperature).

3) LOAD CHANGE

During the sudden load outage from the AC grid under normal grid voltage creates the power imbalance between the incoming HVDC link power and consumption. Hence, the difference power is diverted to flywheel energy storage by the control action presented in Fig 2(c). The difference is used as a reference power command for the GSC. The power injection by the GSC into the DC link raises the DC link voltage. The DC link voltage regulators (PI controller) as shown in Fig. 2(d) processes the DC link voltage deviation that generates the reference quadrature axis current (I_{q-ref}) or electromagnetic torque controlling current for the PMSM coupled flywheel. Finally, the speed of the flywheel is increased, which stores the excess energy from HVDC link due to sudden load change.

D. FLYWHEEL MODEL

The kinetic energy stored in the flywheel is a function of its moment of inertia J (kgm^{-2}) and the square of angular velocity ω (rad/sec) [79]. The moment of inertia of a flywheel is a design parameter that depends on the flywheel mass m (kg) and geometry. For safe operation, the angular velocity of the flywheel ω_{fw} is limited to a minimum (ω_{min}) and maximum (ω_{max}) value [80].

Kinetic energy stored in flywheel is given below,

$$E_{fw} = \frac{1}{2} J\omega^2 \tag{4}$$

Inertia constant of flywheel,

$$H_{fw} = \frac{E_{fw}}{MVA_{rated}} \text{MWs/MVA}$$

Available energy (Watt-hour) in a flywheel,

$$E_{fw(available)}(Wh) = \frac{1}{3600}\left(\frac{1}{2} J\omega_{max}^2 - \frac{1}{2} J\omega_{min}^2\right) \tag{5}$$

The state of energy (SOE_{fw}) of a flywheel defines the amount of kinetic energy that is stored/delivered during its charge/discharge period. It is given by the following equation at time t [80].

$$\begin{aligned} SOE_{fw}(t) &= SOE_{fw}(t - \Delta T) - \frac{\Delta T}{3600 \times E_{max}}\left(\frac{P_{fw}}{\eta_{fw}} + K_{fr}\omega\right) \\ &= SOE_{fw}(t - \Delta T) - E_{con} \end{aligned} \tag{6}$$

where, K_{fr} is the coefficient of friction, P_{fw} is the flywheel incoming/outgoing power, E_{max} is the maximum kinetic energy at maximum angular velocity (ω_{max}), ΔT is the simulation time step, and η_{fw} is the flywheel efficiency. The maximum velocity defines the maximum energy content of the flywheel, E_{max} which corresponds with a state of energy (SoE) equal to 1. The SOE will increase/decrease based on the direction of the flywheel power during charge/discharge operation. Either flywheel delivers energy or not, its energy content, E_{con}, will decrease due to the friction coefficient, K_{fr}. The inertia constant is the ratio of kinetic energy stored at the rated speed to the generator MVA rating, which implies the duration of the generator could generate at its rated power using only its stored rotational kinetic energy. The generator rating is 2MVA and the combined inertia constant is 3.5MWs/MVA. Therefore, flywheel energy storage can deliver 2MW of power in 1.5 seconds from its stored kinetic energy at rated speed. 3.5MWs is equivalent to 0.972kWh. The flywheel's capacity to absorb extra energy from a fast change in load relies on the flywheel current speed, load change duration, and amount, and converter's limit. When operating at or close to its rated maximum speed, a flywheel cannot absorb the extra energy brought on by a sudden change in load. The transient fault is a short-lived problem that minimally alters the speed. A discharging action that can reduce the flywheel energy to a minimum limit during fluctuations in renewable energy sources. Therefore, it depends on the required intermittent renewable energy, converter limits and current flywheel speed. Since the transient faults are small duration faults that changes the small amount of flywheel

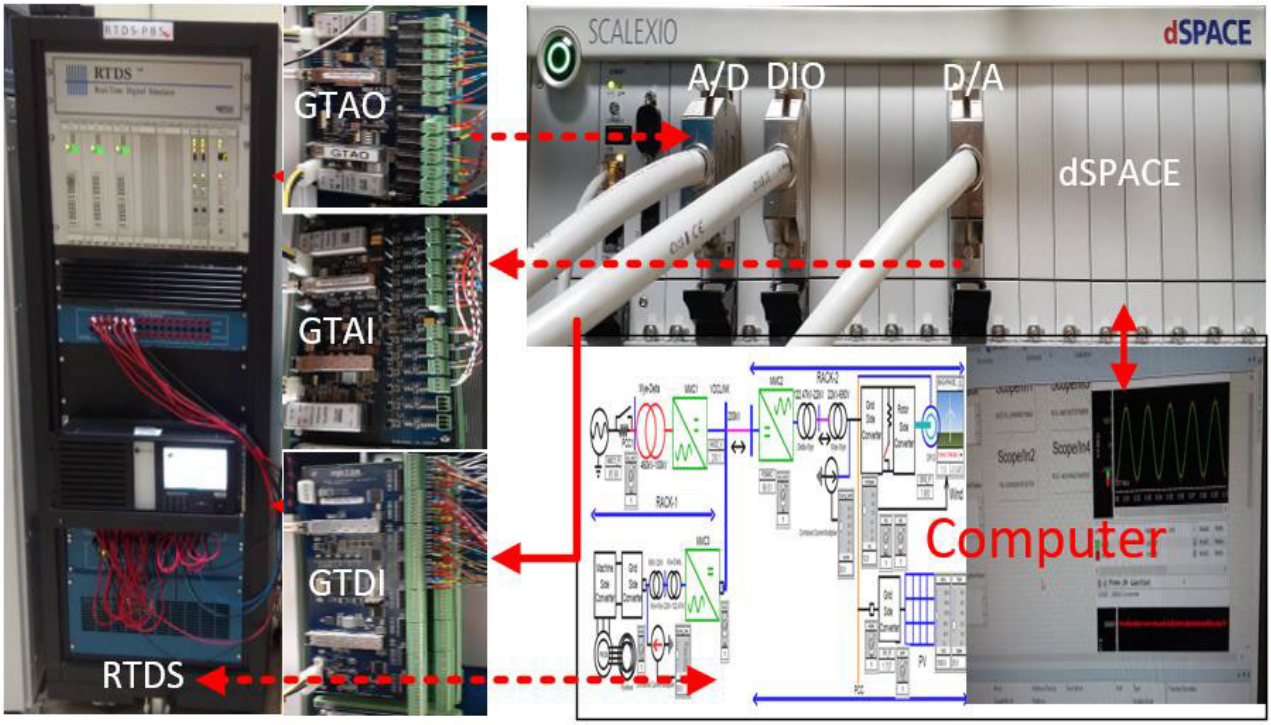

FIGURE 3. dSPACE-SCALEXIO-RTDS interface.

speed due to the absorption of excess energy from the HVDC link, the capacity of flywheel energy storage system can be made smaller compared to the total renewable energy. However, the capacity needs to be enlarged if it is required to support intermittent caused by the renewable energy and load change. In conclusion, the size of the flywheel can vary based on required support.

III. RESULT AND DISCUSSION

The sample time for MMC controller is 100μs. However, the sample time for PV, Wind, and Flywheel controller is 50μs. A multi-rack RTDS platform was used to create the complete system because of the complexity of the system. Nova Core and PB5 CPUs made up the hardware platform used by the RTDS multi-rack. While the Rack-1 has MMC1, MMC3 with flywheel, the Rack-2 has MMC2 with PV and Wind. The MMC1 controller was implemented using the dSPACE-SCALEXIO controller. Fig. 3, Fig. 4, and Fig. 5 depict, respectively, the dSPACE-RTDS hardware setups, MMC1 controller signal in the dSPACE controller, and RTDS runtime interface. Scaling the PCC terminal input current from a complete 1.74 MW PV array and a single 2 MW wind generator unit allowed for the modeling of a 200 MW (megawatts) PV-Wind system. Similar to that, a 200MW flywheel energy storage system was created by scaling a 2MW and 3.5MWs/MVA PMSM based system. The appendix's Table 1 to Table 3 contains all the necessary details about the MMC-HVDC-flywheel energy storage system that was employed in this article. The result of this section is organized as follows. Surplus energy management employing flywheel energy storage system during low voltage faults at the point of common coupling of MMC1 is described in section III-A. Solar and wind energy intermittency improvement are presented in section III-B, and section III-C. Excess energy absorption due to sudden load change is illustrated in section III-D. Section III-E presents the limitation of flywheel energy management system.

A. HVDC-LINK VOLTAGE CONTROL DURING LOW VOLTAGE FAULTS AT PCC1

Power system network is large complex network and subject to low voltage faults. During low voltage, the power transfer capacity of the converter is reduced significantly, which in turns rises the HVDC link voltage. Therefore, proper protection scheme is required to control the surplus energy for the HVDC voltage regulation. Traditionally, dynamic braking resistor based traditional controller for the HVDC link voltage regulation during low voltage faults is used to dissipate the excess energy in the HVDC link. Proposed work controls the HVDC link voltage without the DBR. The severe balanced and unbalanced faults were applied at PCC1 to test the flywheel energy storage controller's efficacy in controlling the HVDC-link voltage within the threshold for the PV-wind coupled MMC-HVDC network. During the fault at PCC1, the flywheel energy storage absorbed the surplus energy from the HVDC-link while PV and wind generation were unaffected. As shown in Fig. 6, a 500ms duration single line to ground fault (LG), double line to ground fault (LLG) and three phase to ground fault (LLLG) is introduced to PCC1 at 0.7s, 1.6s and 2.6s respectively. The PCC1 voltage is decreased by 80% during these faults. During the three-phase to ground faults at PCC1, real power of MMC1 is decreased to a minimum,

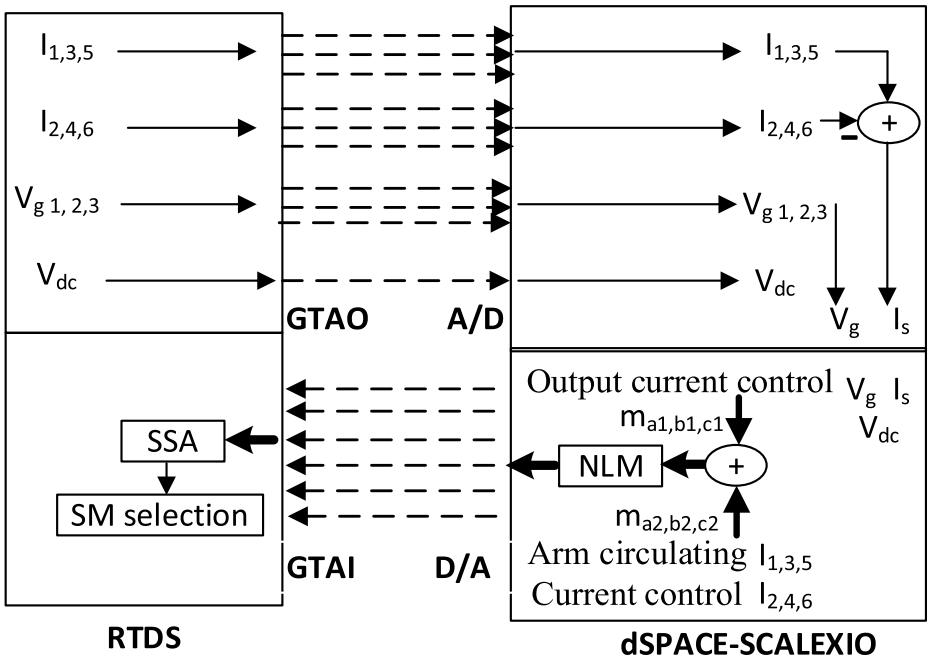

FIGURE 4. Signal exchanged between RTDS and dSPACE-SCALEXIO for MMC1 controller.

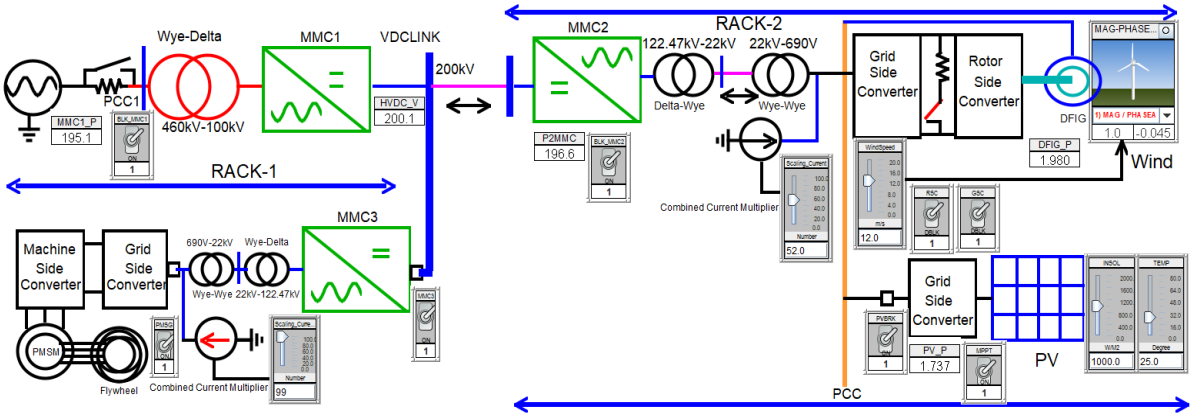

FIGURE 5. Real-time user interfaces in RTDS.

as seen in Fig. 7. The average power delivered during single line to ground fault remains almost same, which did not introduce overvoltage in the HVDC link. Hence, no excess power has been transferred to PMSM, as depicted in Fig. 8. However, reduction in delivered power during LLG and LLLG introduced overvoltage in the HVDC link. Consequently, surplus energy is transferred from HVDC link to PMSM, as illustrated in Fig. 8. As can be seen from Fig. 7, reactive power has been injected into PCC1 for SLG, LLG, and LLLG faults. When the HVDC link voltage exceeds 1.1pu, the difference generates the reference power command for the GSC in power tracking mode according to proposed control strategy. Fig. 7 and Fig. 8 illustrate that the HVDC link voltage rise above 1.1pu resulted in power injection into flywheel during the LLG and LLLG occurrence. Around 0.35MW and 0.75MW peak power was generated as the reference power command for the one-unit GSC. The actual power tracks the reference power. Fig. 9 illustrates that this power is injected into DC link capacitor of GSC, which increases the voltage. The DC link voltage controller of PMSM transfers the DC link voltage error into the electromagnetic torque controlling current that results in speeding up the flywheel. As can be seen from Fig. 8, that speed of flywheel increases from 0.51pu to 0.52pu during LLG, whereas it is increased from 0.52pu to 0.562pu during LLLG. The current controller for both GSC and PMSM confirms the tracking of reference current. In addition, the reactive current for GSC and magnetization current for PMSM are regulated to zero. Due to control action, the HVDC link voltage remains regulated throughout the LG, LLG, and LLLG low voltage severe faults.

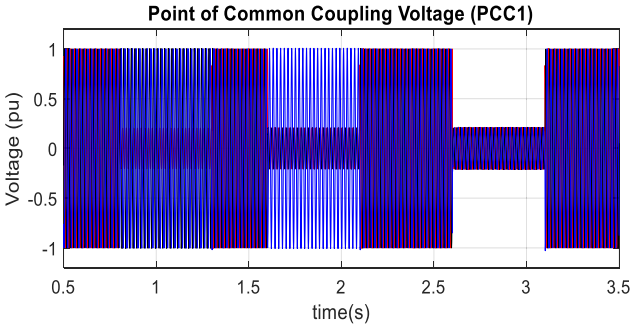

FIGURE 6. 80% voltage drop at PCC1 during SLG, LLG, and LLLG low voltage faults.

Similarly, a 500ms duration single line to ground fault (LG), double line to ground fault (LLG) and three-phase to ground fault (LLLG) is introduced to PCC1 at 0.7s, 1.6s and 2.6s respectively, as depicted in Fig. 11. However, the PCC1 voltage is decreased by 50% during these faults. As can be seen from Fig. 12, both LG and LLG faults have not introduced overvoltage above 1.1pu. Hence, no excess power has been transferred to PMSM during LG and LLG faults, as depicted in Fig. 13. However, reduction in delivered power during LLLG introduced overvoltage above 1.1pu in the HVDC link. Consequently, surplus energy is transferred from HVDC link to PMSM, as illustrated in Fig. 13. As can be seen from Fig. 12, reactive power has been injected into PCC1 for SLG, LLG, and LLLG faults. According to Fig. 13, around 0.3MW peak power was generated as the reference power command for the one-unit GSC. The actual power tracks the reference power. Due to injected power into flywheel, its speed is increased from 0.815pu to 0.821pu. The proposed control action regulated the HVDC link voltage below 1.2pu throughout the LG, LLG, and LLLG low voltage faults.

In addition, a 500ms duration line to line fault (LL), is introduced to PCC1 at 0.7s, as depicted in Fig. 14. However, the PCC1 voltage reduction is not symmetrical, and decreased by 40% to 70% during this fault. As can be seen from Fig. 15, the delivered average real power by MMC1 is reduced from 200MW to 150MW. The reduction in delivered power introduced overvoltage in the HVDC link. Consequently, surplus energy is transferred from HVDC link to PMSM, as illustrated in Fig. 16. When the HVDC link voltage exceeds 1.1pu, the difference generates the reference power command for the GSC in power tracking mode according to proposed control strategy. Around 0.28MW peak power was generated as the reference power command for the one-unit GSC. The actual power tracks the reference power, as depicted in Fig. 16. Fig. 17 illustrates that this power is injected into DC link capacitor of GSC, which increases the voltage. The DC link voltage controller of PMSM transfers the DC link voltage error into the electromagnetic torque controlling current that results in speeding up the flywheel. As can be seen from Fig. 16, that speed of the flywheel is increased from 0.562pu to 0.568pu. The current controller for both GSC and PMSM, as presented in Fig. 17 and Fig. 18 confirms the tracking

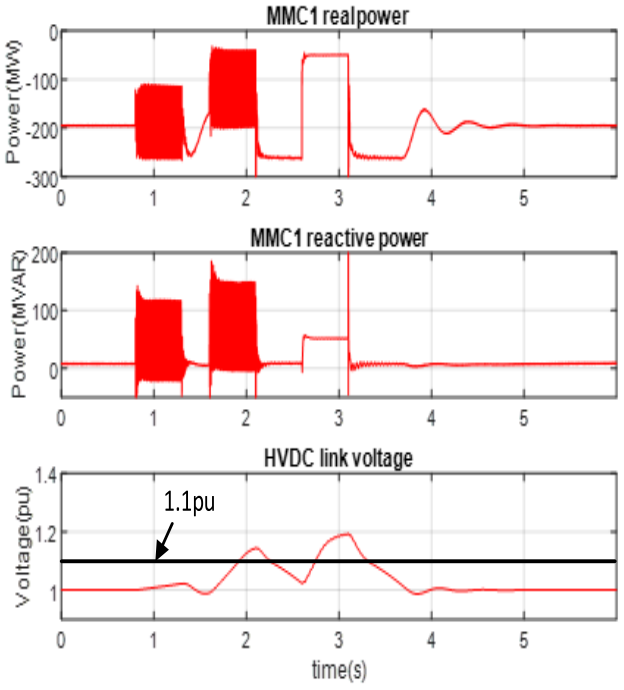

FIGURE 7. Real power, reactive power, and HVDC link voltage of MMC1 during SLG, LLG, and LLLG low voltage faults.

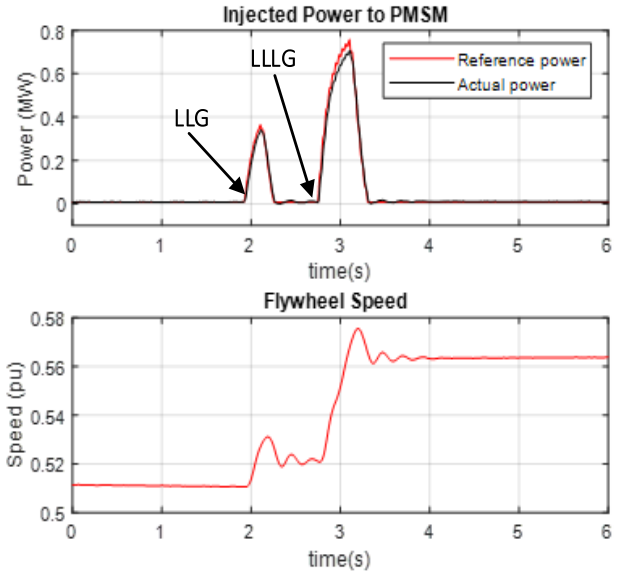

FIGURE 8. Injected power to PMSM and flywheel speed during SLG, LLG, and LLLG low voltage faults.

of reference current. In addition, the reactive current for GSC and magnetization current for PMSM are regulated to zero. Due to control action, the HVDC link voltage remains regulated throughout this fault.

B. POWER SMOOTHING FOR PV SYSTEM UNDER SOLAR IRRADIANCE AND TEMPERATURE CHANGE

To test the flywheel controller's efficacy under renewable energy intermittent, solar irradiance was reduced from

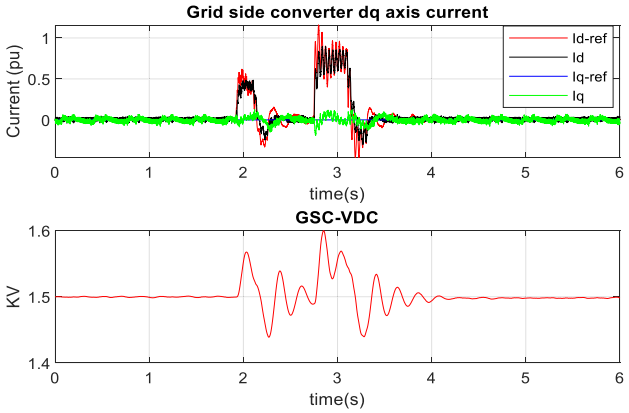

FIGURE 9. Performance of grid side current controller during SLG, LLG, and LLLG low voltage faults.

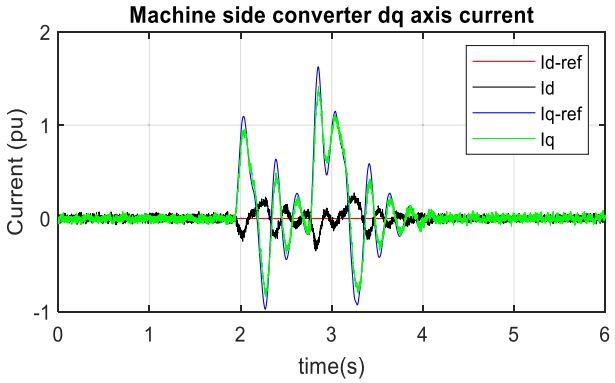

FIGURE 10. Performance of machine side current controller during SLG, LLG, and LLLG low voltage faults.

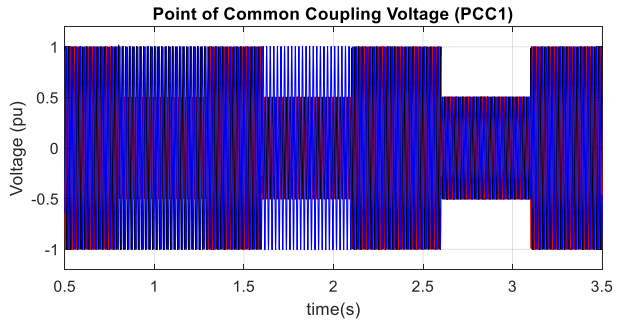

FIGURE 11. 50% voltage drop at PCC1 during SLG, LLG, and LLLG low voltage faults.

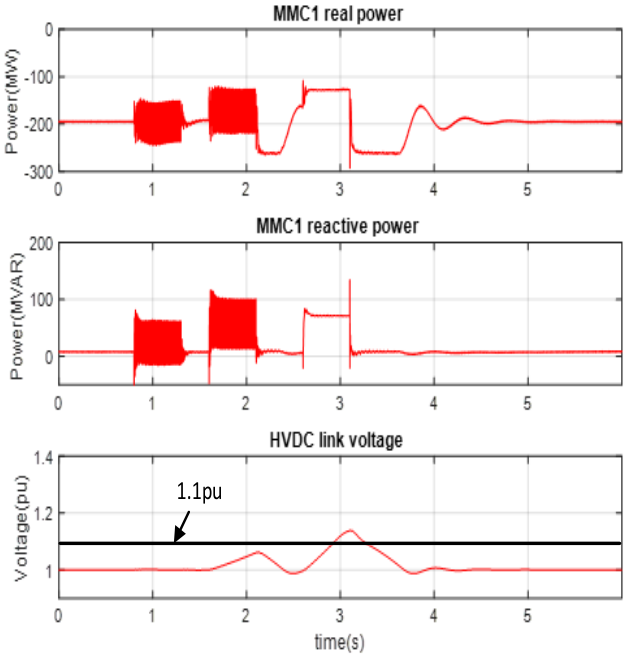

FIGURE 12. Real power, reactive power, and HVDC link voltage of MMC1 during SLG, LLG, and LLLG low voltage faults.

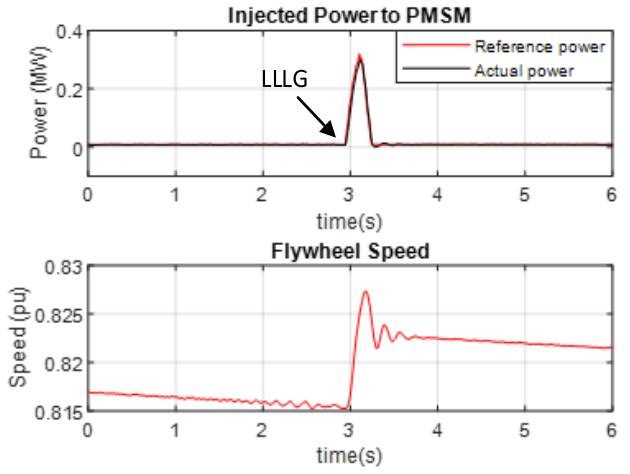

FIGURE 13. Injected power to PMSM and flywheel speed during SLG, LLG, and LLLG low voltage faults.

1000 Wm^{-2} to 200 Wm^{-2}. As shown in Fig. 19, the flywheel compensated for the PV power deficit caused by reduced solar radiation. Due to solar radiation change, the combined PV and Wind power was reduced from around 200MW to around 125MW. During this time, power from flywheel energy storage was increased from 0MW to 75MW through the MMC3, which in turn kept the MMC1 power delivery almost constant. Likewise, when solar radiation was changed from 200 Wm^{-2} to 1000 Wm^{-2}, the injected power from flywheel energy storage dropped from 75 MW to zero, as seen in Fig. 19. As a result, the combined PV and Wind power returned from 125MW to around 200MW. During the transient, real power delivered by the MMC1 did not experience any overshoot. Similarly, HVDC link voltage remains almost constant. As can be seen from Fig. 20, the actual power tracks the reference power. The flywheel speed dropped from 0.95pu to 0.58pu during this discharge period, as depicted in Fig. 20. The flywheel discharge rate is high during the large change of power. According to the control strategy proposed in Fig. 2(b), any deviation from the nominal power

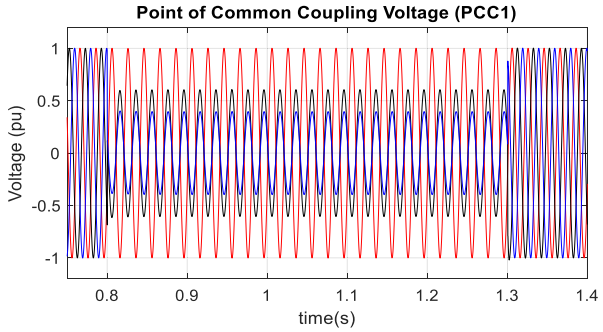

FIGURE 14. Voltage at PCC1 during LL fault.

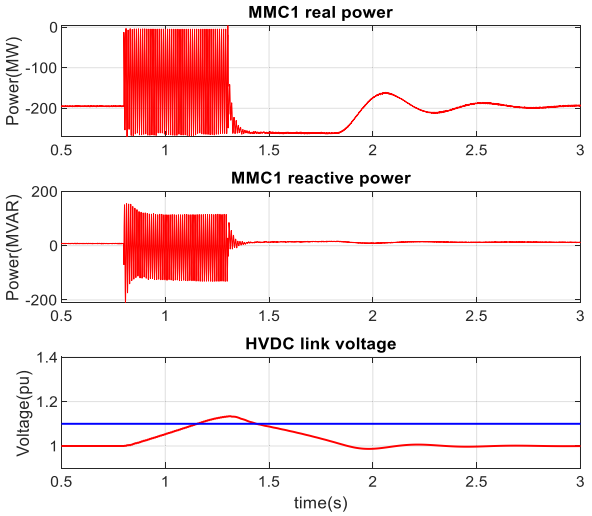

FIGURE 15. Real power, reactive power, and HVDC link voltage of MMC1 during LL faults.

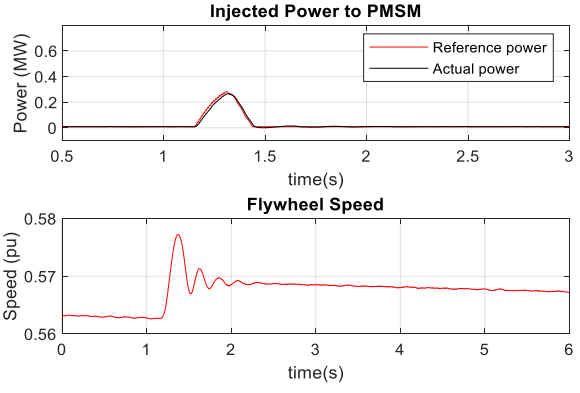

FIGURE 16. Injected power to PMSM and flywheel speed during LL faults.

is compensated by the flywheel energy storage. GSC transfers power from flywheel energy storage to HVDC link through the MMC3. Hence, DC link voltage of GSC is reduced, as depicted in Fig. 21. The DC link voltage regulators (PI controller) as shown in Fig. 2(d) processes the DC link voltage deviation that generates the reference quadrature axis

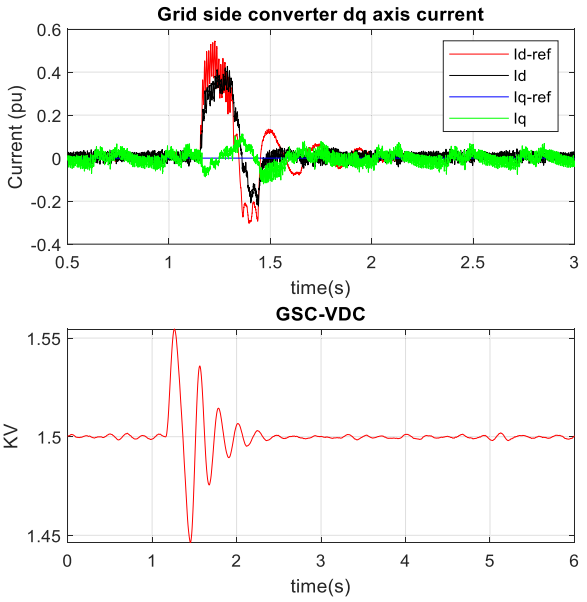

FIGURE 17. Performance of grid side current controller during LL faults.

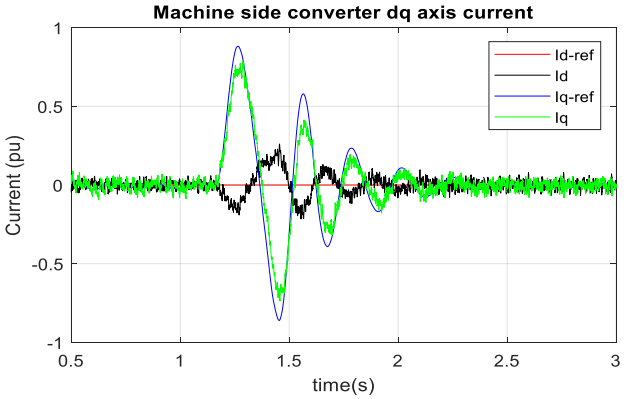

FIGURE 18. Performance of machine side current controller during LL faults.

current (I_{q-ref}) for the PMSM coupled flywheel. The electromagnetic torque is negative, which operates the PMSM as generator by slowing down the speed. Fig. 21, and Fig. 22 show that the actual current follows the commanded current for GSC and PMSM. Fig. 23 shows that the flywheel energy storage compensated for the PV power fluctuation induced by temperature variation. As shown in Fig. 23, the temperature was increased from 25 to 45 degrees Celsius, lowering the combined PV and wind power output to around 192 MW from around 200 MW. As a result, the power injected from the flywheel energy storage was raised to 8 MW from zero to compensate for the deficit, keeping the MMC1 supplied power constant. Similarly, during the temperature drop from 45^0C to 25^0C, flywheel energy storage power was lowered to zero from 8 MW. During such a transition, the real power delivered by the MMC1 did not experience any overshot. In addition, HVDC link voltage remains regulated. Fig. 24

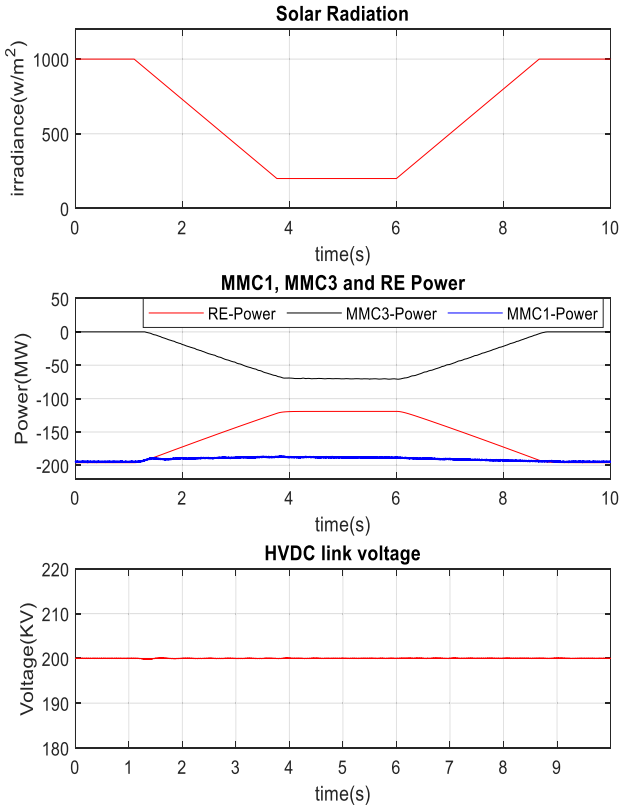

FIGURE 19. Solar Irradiance, Real power change of PV-Wind, MMC3 and MMC1, and HVDC link voltage.

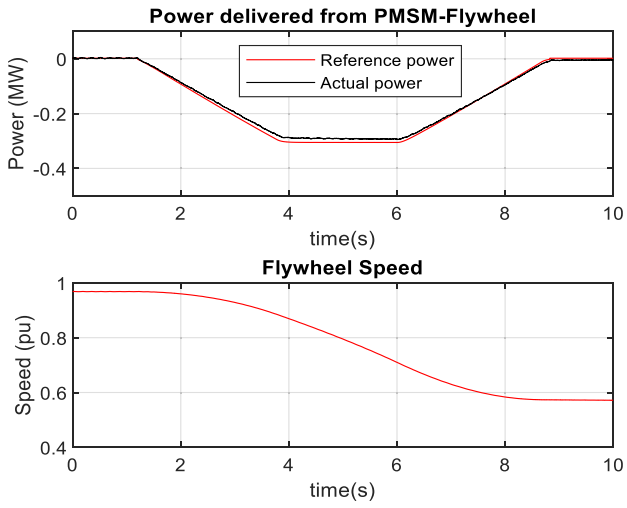

FIGURE 20. Delivered power from PMSM-Flywheel and Flywheel speed during solar radiation change.

shows the delivered power from one flywheel energy storage and the speed change of flywheel. For the small change of power due to temperature change, the speed of flywheel dropped from 0.97pu to 0.95pu. The commanded reference power is tracked by the actual power, as depicted in Fig. 24.

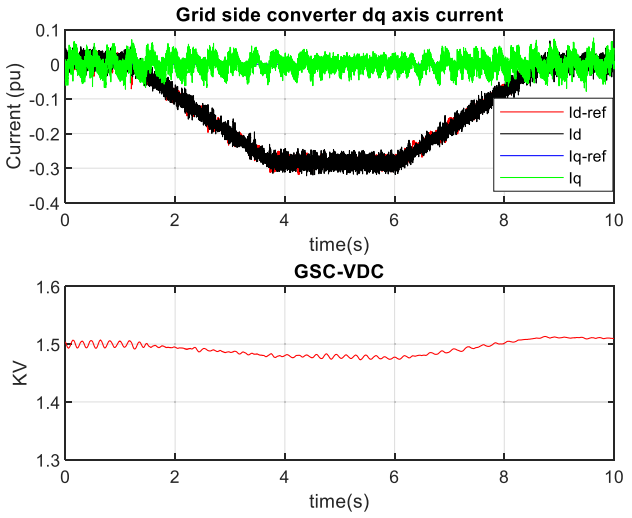

FIGURE 21. Performance of grid side converter during solar radiation change.

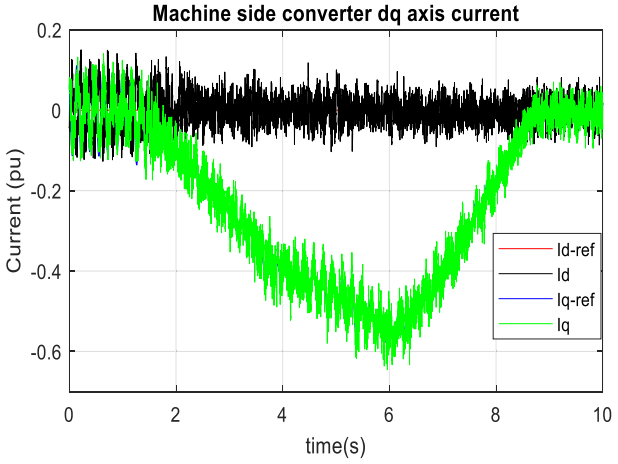

FIGURE 22. Performance of machine side converter during solar radiation change.

C. FLYWHEEL-BASED POWER SMOOTHING UNDER WIND SPEED VARIATION

To test the flywheel energy storage controller's efficacy, the wind speed was varied from 12 ms^{-1} to 8 ms^{-1}. The flywheel energy storage compensated for the reduced power due to the lower wind speed, as shown in Fig. 25. Due to wind speed change, the combined PV and Wind power was reduced from around 200MW to around 150MW. During this time, power from flywheel energy storage was increased from 0MW to 50MW through the MMC3, which in turn kept the MMC1 power delivery almost constant. Likewise, when wind speed was changed from 8 ms^{-1} to 12 ms^{-1}, the injected power from flywheel energy storage dropped from 50 MW to zero, as seen in Fig. 25. As a result, the combined PV and Wind power returned from 150MW to around 200MW. During the transient, real power delivered by the MMC1 did

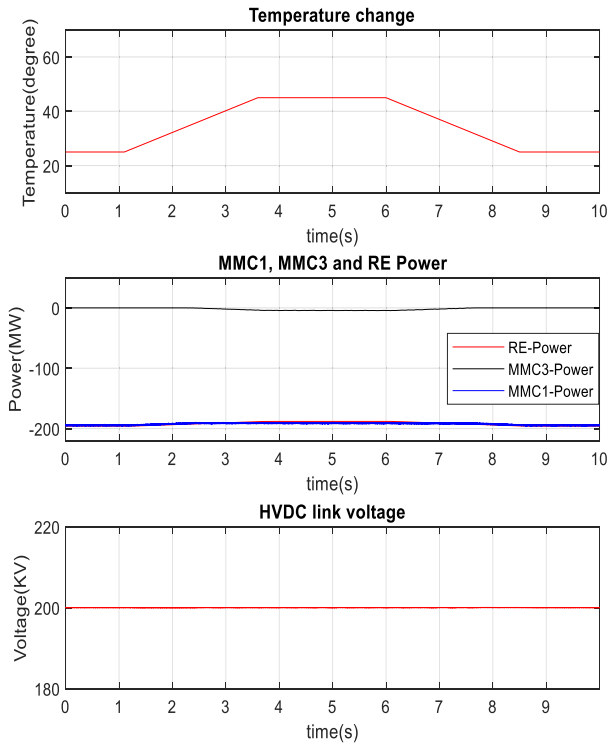

FIGURE 23. PV Temperature, Real power change of PV-Wind, MMC3 and MMC1, and HVDC link voltage.

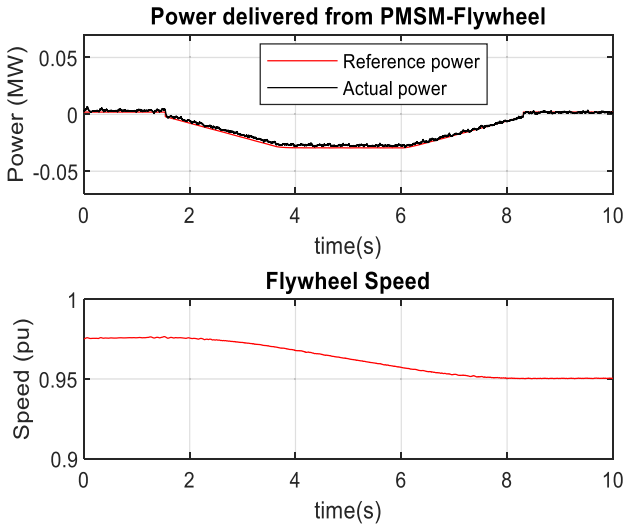

FIGURE 24. Delivered power from PMSM-Flywheel and Flywheel speed during PV temperature change.

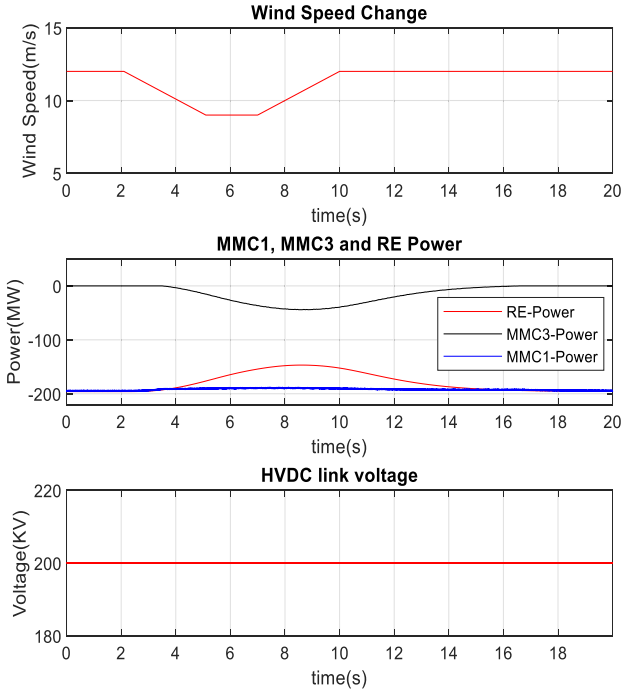

FIGURE 25. Wind speed, Real power change of PV-Wind, MMC3 and MMC1, and HVDC link voltage.

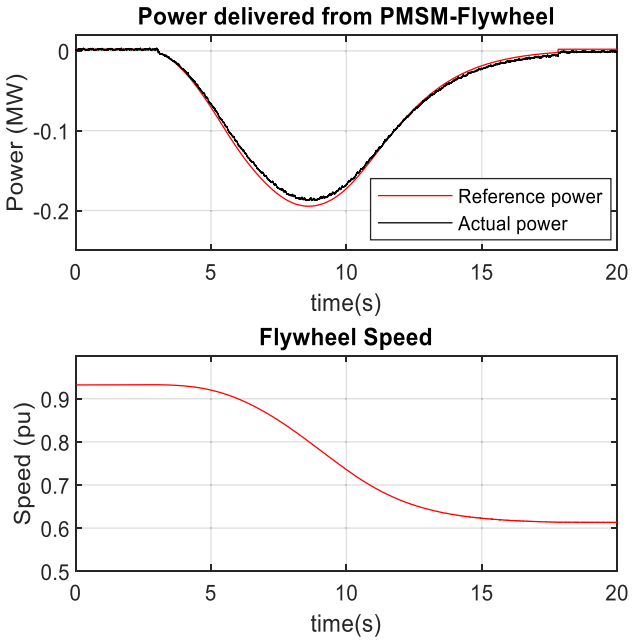

FIGURE 26. Delivered power from PMSM-Flywheel and Flywheel speed during wind speed change.

not experience any overshoot. Similarly, HVDC link voltage remains almost constant. As can be seen from Fig. 26, the actual power tracks the reference power. The flywheel speed dropped from 0.91pu to 0.61pu during this discharge period, as depicted in Fig. 26. The discharge rate of flywheel is high during the large change of power. According to the control strategy proposed in Fig. 2(b), any deviation from the nominal power is compensated by the flywheel energy storage. GSC transfers power from flywheel energy storage to HVDC link through the MMC3. Hence, DC link voltage of GSC is reduced, as depicted in Fig. 27. The DC link voltage regulators (PI controller) as shown in Fig. 2(d) processes the DC link voltage deviation that generates the reference electromagnetic torque controlling current for the PMSM

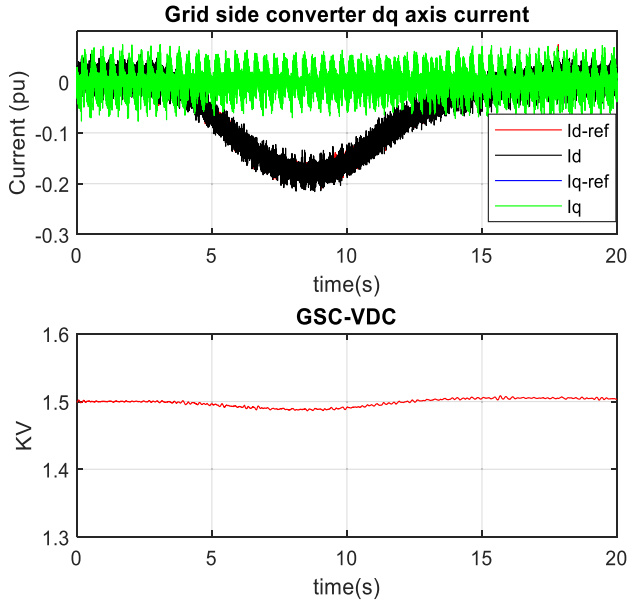

FIGURE 27. Performance of grid side converter during wind speed change.

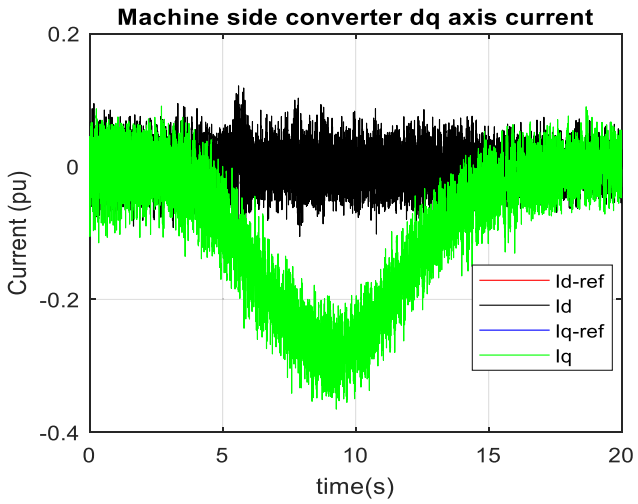

FIGURE 28. Performance of machine side converter during wind speed change.

coupled flywheel. The electromagnetic torque is negative, which operates the PMSM as generator by slowing down the speed. Fig. 27, and Fig. 28 show that the actual current follows the commanded current for GSC and PMSM. During the transient, the MMC1 provided nominal real power and did not experience any overshooting as the flywheel energy storage controller effectively responded to the change in the wind farm due to wind speed variation.

D. FLYWHEEL-BASED POWER SMOOTHING UNDER LOAD VARIATION

In this section, the solar radiation for the PV system and the wind speed for the wind farm were constant, whereas the

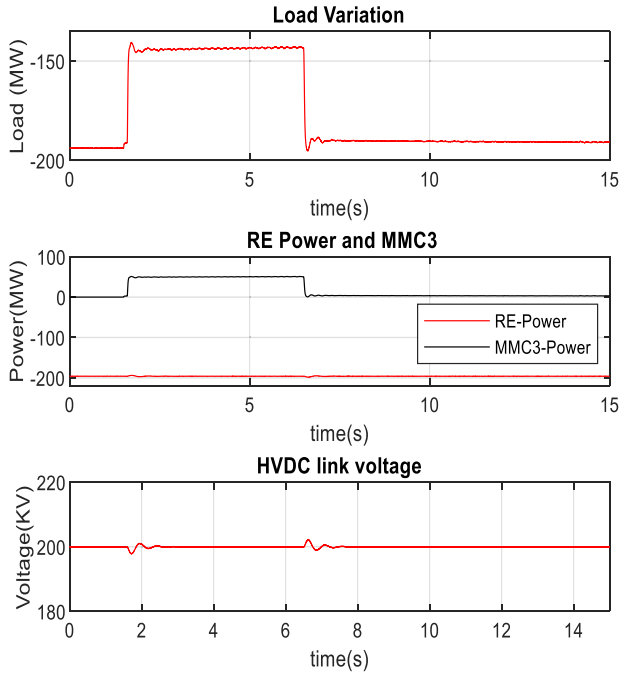

FIGURE 29. Load power change, Renewable Energy (RE) power, and the power of MMC3, and HVDC link voltage.

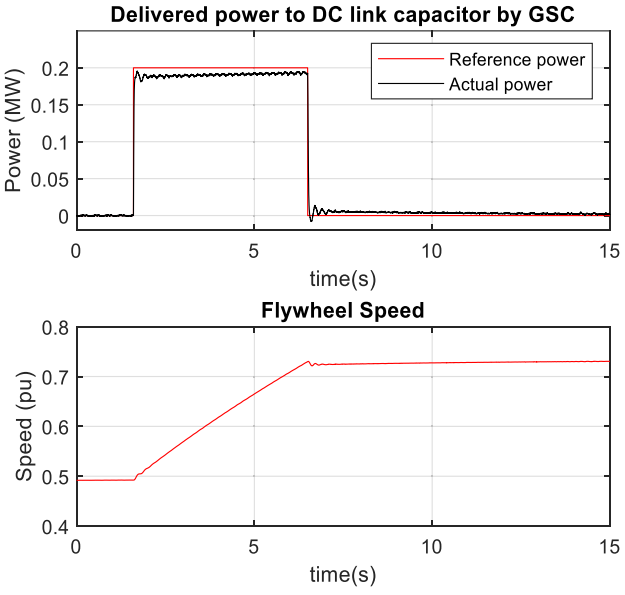

FIGURE 30. Injected power into DC link capacitor of GSC and Flywheel speed during load change.

load on the AC grid was suddenly changed from 190MW to 140MW to test the effectiveness of the flywheel-based power smoothing controller under sudden load variation. As can be seen from Fig. 29, the combined solar and wind energy remains constant, and the excess energy in the DC link due to sudden load change is transferred to flywheel energy storage through the MMC3. Around 50MW was injected

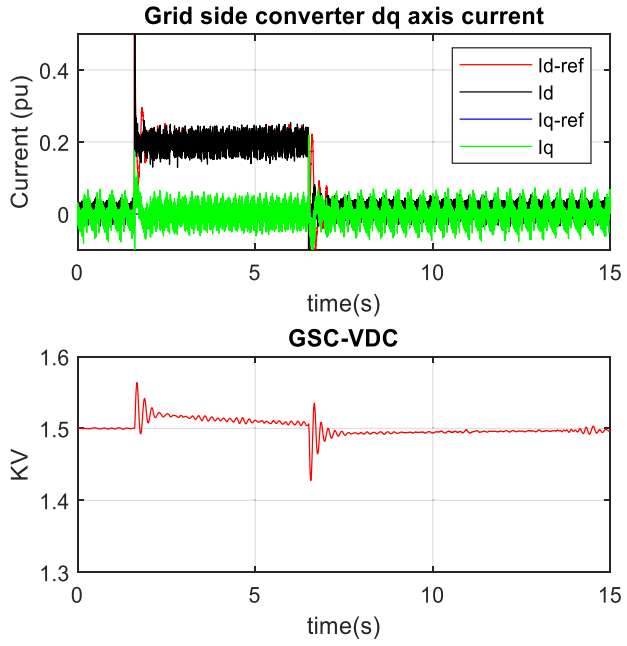

FIGURE 31. Performance of grid side converter during load change.

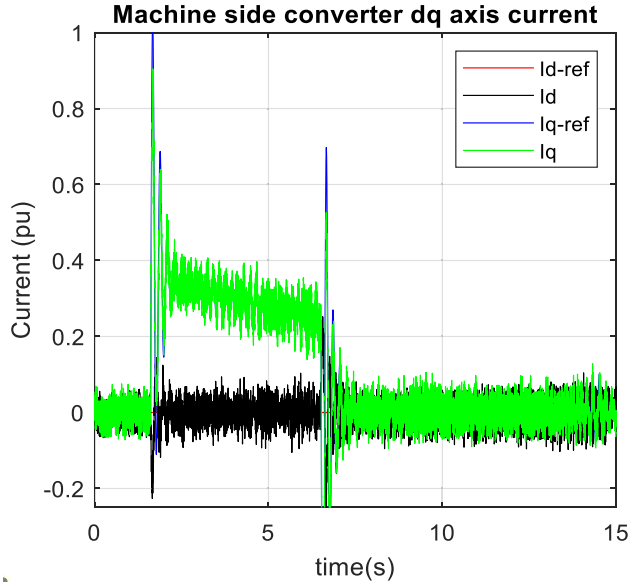

FIGURE 32. Performance of machine side converter during load change.

into flywheel energy storage. Small overshot was introduced into the HVDC link voltage at the start and end of the load transient. During the sudden load outage from the AC grid under normal grid voltage creates the power imbalance between the incoming HVDC link power and consumption. Hence, the difference power is diverted to flywheel energy storage by the control action presented in Fig. 2(c). The difference is used as a reference power command for the GSC. Fig. 30 shows that the actual power of GSC tracks the commanded reference power generated by the control action presented in Fig 2(c). The power injection by the GSC into the DC link raises the DC link voltage, as depicted in Fig. 31. The DC link voltage regulators (PI controller) as shown in Fig. 2(d) processes the DC link voltage deviation that generates the reference quadrature axis current (I_{q-ref}) for the PMSM coupled flywheel. Finally, the speed of the flywheel is increased, which stores the excess energy from HVDC link. Thus, HVDC link voltage remains within the threshold. The flywheel speed is increased from 0.49pu to 0.72pu due to power injection into flywheel, as shown in Fig. 30. Fig. 31, and Fig. 32 show that the actual current follows the commanded current for GSC and PMSM.

E. LIMITATION OF FLYWHEEL ENERGY STORAGE

Although flywheel has the ability to absorb excess energy from the sudden load change, it depends on its current speed, load power change and duration. If it is already near its rated maximum speed, it cannot absorb the excess energy due to load change. However, the transient fault is small duration faults that change the speed minimally as illustrated in section III-A. Power smoothing control during renewable energy fluctuation is a discharging action that can discharge the flywheel energy to a minimum limit. Therefore, its duration depends on its current speed and required intermittent renewable energy. In summary, the following are the limitations of flywheel energy storage.

1) It cannot absorb the excess energy caused by a quick load shift if it is already operating at close to its rated maximum speed.
2) If it is already close to its minimal speed, it cannot provide the necessary energy during the variation in renewable energy.
3) Self-discharge due to rotational friction loss that reduces the flywheel speed over time.

However, due to a slight change in flywheel speed, it can absorb extra energy from the HVDC link during transient low voltage disturbances at the AC side of MMC1. These limitations are not only the case for flywheel energy storage system, but any other energy storage system is also similarly subject to the aforementioned limitations. Flywheels have a high number of charging and discharging cycles, however before choosing flywheel energy storage system over another type of energy storage system, it is important to carefully consider its maintenance and operation expenses as well as self-discharge loss. New, innovative designs, recyclable and durable materials, reduced mechanical (drag, bearing, friction), electrical (hysteresis, eddy current, copper), and power converter-related (switching and conduction) losses can improve the overall prospect of flywheel energy storage system, and make economically competitive [61].

IV. CONCLUSION

To successfully regulate the HVDC-link surplus power and maintain the HVDC link voltage within the limit during

TABLE 1. PV module, Wind turbine, DFIG wind generator and converter data.

PV module and array parameters		Wind turbine parameters	
Quantity	Value	Quantity	Value
Cells per module	36	Nominal wind speed	12 m/s
Short circuit current	3.35 A	Nominal generator speed, DFIG	1.2 pu
Open circuit voltage	21.7 V	Nominal turbine power	2 MW
Current at MPP	3.05 A	**DFIG parameters**	
Voltage at MPP	17.4 V	Quantity	Value
Temperature coefficient of I_{sc}	0.065 %/degree	Stator voltage (L-L)	690 V
Temperature coefficient of V_{oc}	-0.56 %/degree	Nominal frequency, f	50 Hz
Series connected modules per string	115	Nominal power	2.2 MVA
Parallel strings	285	Stator resistance, R_s	1 mΩ
		Rotor resistance, R_r	1.3 mΩ
Grid side VSC parameters for PV/DFIG		Inductance of stator, L_s	2.55 mH
Quantity	Value	Inductance of rotor, L_r	2.56 mH
Nominal DC-link voltage	2 kV	Magnetizing inductance, L_m	2.44 mH
Rated power	2.2 MVA	**Filter parameters (R_F// L_F + C_F)**	
Resistance, R	0.004 pu	Filter inductance, L_F	4.3 µH
Inductance, L	0.15 pu	Filter capacitance, C_F	1.47 mF
M11	52	Filter resistance, R_F	0.054 Ω

TABLE 2. PMSM Flywheel Parameters.

PMSM Parameters		Flywheel Parameters	
Quantity	Value	Quantity	Value
Stator voltage (L-L)	0.69kV	Power Rating	2MW
PMSM nominal power	2MW	Inertia Constant, H	3.5 MWs/MVA
		K_{fr}, coefficient of friction	0.3
		Efficiency, η_{fw}	90%
Number of pole pairs	8	**Grid side VSC parameters**	
Nominal frequency of PMSG	3.77 Hz	Quantity	Value
Stator resistance	2 21mΩ	DC link Voltage	1.5kV
d and q axis inductance (L_d and L_q)	9.816mH	DC link capacitor	5500µF
Flux linkage established by magnets, λ_m	7.0304 Vs	Rated power	2.5 MVA
PI_1	(0.4+1/s) pu	Rated voltage	0.69kV
M12	99	Resistance, R	0.004 pu
		Inductance, L	0.15 pu

TABLE 3. MMC and battery controller parameters.

Parameters	Value	Parameters	Value
Rated power	250 MW	C	16 mF
Rated HVDC-link voltage	200 kV	C_d	100 µF
Rated AC voltage(L-L)	100 kV	SM/arm	200
Nominal frequency	50 Hz	DC line resistance per km	1.39 mΩ
Reactor resistance, R	0.002 pu	DC line inductance per km	0.159 mH
Reactor inductance, L	0.2 pu	DC line capacitance per km	0.231 µF
Modulation	Nearest level		
AC grids' short circuit ratio	10		

the low voltage disturbance at the PCC1 of the AC grids, a flywheel energy storage-based control approach was developed. Another control method was also developed to smooth out power variations brought on by changes in temperature, wind speed, solar radiation, and load. By linking the dSPACE controller with the RTDS hardware and creating the controller hardware in a loop arrangement for the complete system, including all switching converter models, it was simulated and tested in real-time. The results validate the proposed power smoothing control technique for the flywheel energy storage system to maintain the HVDC-link voltage during low voltage disturbances and enhance transient performance during variations in renewable energy and load. Furthermore, the controller improved the low voltage fault ride-through capability of the MMC-HVDC system by delivering reactive power at the point of common coupling of AC grids during symmetrical and unsymmetrical low voltage faults. For the fast frequency regulation of AC grids, a combination of renewable energy and flywheel energy storage can be examined as further research. In addition, it can be further investigated with conventional power plants for boosting energy production during peak demand. The battery or hydrogen fuel cell can also be added to the proposed renewable energy-connected MMC-HVDC system for investigating fault ride-through capability and intermittent renewable energy support.

APPENDIX

See Tables 1–3.

REFERENCES

[1] M. I. Hossain and M. A. Abido, "SCIG based wind energy integrated multiterminal MMC-HVDC transmission network," *Sustainability*, vol. 12, no. 9, p. 3622, Apr. 2020, doi: 10.3390/SU12093622.

[2] M. I. Hossain and M. A. Abido, "Positive-negative sequence current controller for LVRT improvement of wind farms integrated MMC-HVDC network," *IEEE Access*, vol. 8, pp. 193314–193339, 2020, doi: 10.1109/ACCESS.2020.3032400.

[3] M. I. Hossain and M. A. Abido, "Active power control of PV-battery connected MMC-HVDC system for FRT support," *Appl. Sci.*, vol. 10, no. 20, p. 7186, Oct. 2020, doi: 10.3390/APP10207186.

[4] M. Zhang, X. Yuan, and J. Hu, "Inertia and primary frequency provisions of PLL-synchronized VSC HVDC when attached to islanded AC system," *IEEE Trans. Power Syst.*, vol. 33, no. 4, pp. 4179–4188, Jul. 2018, doi: 10.1109/TPWRS.2017.2780104.

[5] J. N. Sakamuri, Z. H. Rather, J. Rimez, M. Altin, O. Goksu, and N. A. Cutululis, "Coordinated voltage control in offshore HVDC connected cluster of wind power plants," *IEEE Trans. Sustain. Energy*, vol. 7, no. 4, pp. 1592–1601, Oct. 2016, doi: 10.1109/TSTE.2016.2569430.

[6] A. Moawwad, M. S. El Moursi, and W. Xiao, "Advanced fault ride-through management scheme for VSC-HVDC connecting offshore wind farms," *IEEE Trans. Power Syst.*, vol. 31, no. 6, pp. 4923–4934, Nov. 2016, doi: 10.1109/TPWRS.2016.2535389.

[7] A. Moawwad, M. S. El Moursi, and W. Xiao, "A novel transient control strategy for VSC-HVDC connecting offshore wind power plant," *IEEE Trans. Sustain. Energy*, vol. 5, no. 4, pp. 1056–1069, Oct. 2014, doi: 10.1109/TSTE.2014.2325951.

[8] A. Egea-Àlvarez, M. Aragüés-Peñalba, E. Prieto-Araujo, and O. Gomis-Bellmunt, "Power reduction coordinated scheme for wind power plants connected with VSC-HVDC," *Renew. Energy*, vol. 107, pp. 1–13, Jul. 2017, doi: 10.1016/J.RENENE.2017.01.027.

[9] M. I. Hossain, M. Shafiullah, F. A. Al-Sulaiman, and M. A. Abido, "Comprehensive analysis of PV and wind energy integration into MMC-HVDC transmission network," *Sustainability*, vol. 15, no. 1, p. 253, Dec. 2022, doi: 10.3390/SU15010253.

[10] M. I. Hossain, M. A. Abido, and M. I. Pathan, "PMSG based wind energy integration into MMC based HVDC transmission network in RTDS," in *Proc. IEEE Electr. Power Energy Conf. (EPEC)*, Nov. 2020, pp. 1–6, doi: 10.1109/EPEC48502.2020.9320059.

[11] M. I. Hossain, M. A. Abido, and M. I. Pathan, "MMC based PV energy integrated multiterminal HVDC transmission network," in *Proc. IEEE Electr. Power Energy Conf. (EPEC)*, Nov. 2020, pp. 1–6, doi: 10.1109/EPEC48502.2020.9320120.

[12] S. Nanou and S. Papathanassiou, "Evaluation of a communication-based fault ride-through scheme for offshore wind farms connected through high-voltage DC links based on voltage source converter," *IET Renew. Power Gener.*, vol. 9, no. 8, pp. 882–891, Nov. 2015, doi: 10.1049/iet-rpg.2015.0017.

[13] M. Ndreko, M. Popov, and M. A. M. M. van der Meijden, "Study on FRT compliance of VSC-HVDC connected offshore wind plants during AC faults including requirements for the negative sequence current control," *Int. J. Electr. Power Energy Syst.*, vol. 85, pp. 97–116, Feb. 2017, doi: 10.1016/J.IJEPES.2016.08.009.

[14] S. I. Nanou, G. N. Patsakis, and S. A. Papathanassiou, "Assessment of communication-independent grid code compatibility solutions for VSC–HVDC connected offshore wind farms," *Electr. Power Syst. Res.*, vol. 121, pp. 38–51, Apr. 2015, doi: 10.1016/J.EPSR.2014.12.002.

[15] M. Mohammadi, M. Avendano-Mora, M. Barnes, and J. Y. Chan, "A study on fault ride-through of VSC-connected offshore wind farms," in *Proc. IEEE Power Energy Soc. Gen. Meeting*, Mar. 2013, p. 1–4, doi: 10.1109/PESMG.2013.6672514.

[16] O. D. Adeuyi, M. Cheah-Mane, J. Liang, L. Livermore, and Q. Mu, "Preventing DC over-voltage in multi-terminal HVDC transmission," *CSEE J. Power Energy Syst.*, vol. 1, no. 1, pp. 86–94, Mar. 2015, doi: 10.17775/CSEEJPES.2015.00011.

[17] O. Gomis-Bellmunt, A. Egea-Alvarez, A. Junyent-Ferre, J. Liang, J. Ekanayake, and N. Jenkins, "Multiterminal HVDC-VSC for offshore wind power integration," in *Proc. IEEE Power Energy Soc. Gen. Meeting*, Jul. 2011, pp. 1–6, doi: 10.1109/PES.2011.6039238.

[18] R. Chen, K. Jia, T. Bi, B. Liu, and Y. Sun, "Coordinated fault ride through strategy for offshore wind integration system," *IOP Conf. Ser. Earth Environ. Sci.*, vol. 170, no. 4, p. 42124, Jul. 2018, doi: 10.1088/1755-1315/170/4/042124.

[19] A. Arulampalam, G. Ramtharan, N. Caliao, J. B. Ekanayake, and N. Jenkins, "Simulated onshore-fault ride through of offshore wind farms connected through VSC HVDC," *Wind Eng.*, vol. 32, no. 2, pp. 103–114, Mar. 2008, doi: 10.1260/030952408784815781.

[20] M. Ndreko, A. Bucurenciu, M. Popov, and M. A. M. M. van der Meijden, "On grid code compliance of offshore MTDC grids: Modeling and analysis," in *Proc. IEEE Eindhoven PowerTech*, Jun. 2015, pp. 1–6, doi: 10.1109/PTC.2015.7232398.

[21] Y. Yu, Z. Xu, and T. An, "Fault ride-through strategy for fully rated converter wind turbines connected to the grid via MMC-HVDC transmission," in *Proc. 12th IET Int. Conf. AC DC Power Transmiss. (ACDC)*, 2016, p. CP696, doi: 10.1049/CP.2016.0406.

[22] J. Liang, O. Gomis-Bellmunt, J. Ekanayake, N. Jenkins, and W. An, "A multi-terminal HVDC transmission system for offshore wind farms with induction generators," *Int. J. Electr. Power Energy Syst.*, vol. 43, no. 1, pp. 54–62, Dec. 2012, doi: 10.1016/j.ijepes.2012.04.063.

[23] W. Sun, R. E. Torres-Olguin, and O. Anaya-Lara, "Investigation on fault-ride through methods for VSC-HVDC connected offshore wind farms," *Energy Proc.*, vol. 94, pp. 29–36, Sep. 2016, doi: 10.1016/J.EGYPRO.2016.09.185.

[24] I. Erlich, C. Feltes, and F. Shewarega, "Enhanced voltage drop control by VSC–HVDC systems for improving wind farm fault ridethrough capability," *IEEE Trans. Power Del.*, vol. 29, no. 1, pp. 378–385, Feb. 2014, doi: 10.1109/TPWRD.2013.2285236.

[25] Y. Jing, R. Li, L. Xu, and Y. Wang, "Enhanced AC voltage and frequency control on offshore MMC station for wind farm," *J. Eng.*, vol. 2017, no. 13, pp. 1264–1268, Jan. 2017, doi: 10.1049/JOE.2017.0532.

[26] U. Karaagac, J. Mahseredjian, L. Cai, and H. Saad, "Offshore wind farm modeling accuracy and efficiency in MMC-based multiterminal HVDC connection," *IEEE Trans. Power Del.*, vol. 32, no. 2, pp. 617–627, Apr. 2017, doi: 10.1109/TPWRD.2016.2522562.

[27] M. C. Nguyen, K. Rudion, and Z. A. Styczynski, "Improvement of stability assessment of VSCHVDC transmission systems," in *Proc. 5th Int. Conf. Crit. Infrastruct. (CRIS)*, Sep. 2010, pp. 1–10, doi: 10.1109/CRIS.2010.5617545.

[28] L. Xu, L. Yao, and C. Sasse, "Grid integration of large DFIG-based wind farms using VSC transmission," *IEEE Trans. Power Syst.*, vol. 22, no. 3, pp. 976–984, Aug. 2007, doi: 10.1109/TPWRS.2007.901306.

[29] X. Hu, J. Liang, D. J. Rogers, and Y. Li, "Power flow and power reduction control using variable frequency of offshore AC grids," *IEEE Trans. Power Syst.*, vol. 28, no. 4, pp. 3897–3905, Nov. 2013, doi: 10.1109/TPWRS.2013.2257884.

[30] B. Silva, C. L. Moreira, H. Leite, and J. A. Pecas Lopes, "Control strategies for AC fault ride through in multiterminal HVDC grids," *IEEE Trans. Power Del.*, vol. 29, no. 1, pp. 395–405, Feb. 2014, doi: 10.1109/TPWRD.2013.2281331.

[31] O. Goksu, R. Teodorescu, C. L. Bak, F. Iov, and P. C. Kjaer, "Instability of wind turbine converters during current injection to low voltage grid faults and PLL frequency based stability solution," *IEEE Trans. Power Syst.*, vol. 29, no. 4, pp. 1683–1691, Jul. 2014, doi: 10.1109/TPWRS.2013.2295261.

[32] M. Aragues Penalba, O. Gomis-Bellmunt, and M. Martins, "Coordinated control for an offshore wind power plant to provide fault ride through capability," *IEEE Trans. Sustain. Energy*, vol. 5, no. 4, pp. 1253–1261, Oct. 2014, doi: 10.1109/TSTE.2014.2344172.

[33] S. Ma, H. Geng, L. Liu, G. Yang, and B. C. Pal, "Grid-synchronization stability improvement of large scale wind farm during severe grid fault," *IEEE Trans. Power Syst.*, vol. 33, no. 1, pp. 216–226, Jan. 2018, doi: 10.1109/TPWRS.2017.2700050.

[34] W. Li, M. Zhu, P. Chao, X. Liang, and D. Xu, "Enhanced FRT and post-fault recovery control for MMC-HVDC connected offshore wind farms," *IEEE Trans. Power Syst.*, vol. 35, no. 2, pp. 1606–1617, Mar. 2020, doi: 10.1109/TPWRS.2019.2944940.

[35] *Battery Storage for Renewables: Market Status and Technology Outlook*. Accessed: Jan. 27, 2022. [Online]. Available: http://publications/2015/Jan/Battery-Storage-for-Renewables-Market-Status-and-Technology-Outlook

[36] *CNESA Global Energy Storage Market Analysis—2020.Q1 (Summary)—China Energy Storage Alliance*. Accessed: Jan. 27, 2022. [Online]. Available: http://en.cnesa.org/latest-news/2020/5/28/cnesa-global-energy-storage-market-analysis-2020q1-summary

[37] M. Y. Suberu, M. W. Mustafa, and N. Bashir, "Energy storage systems for renewable energy power sector integration and mitigation of intermittency," *Renew. Sustain. Energy Rev.*, vol. 35, pp. 499–514, Jul. 2014, doi: 10.1016/j.rser.2014.04.009.

[38] H. Chen, T. N. Cong, W. Yang, C. Tan, Y. Li, and Y. Ding, "Progress in electrical energy storage system: A critical review," *Prog. Natural Sci.*, vol. 19, no. 3, pp. 291–312, Mar. 2009, doi: 10.1016/j.pnsc.2008.07.014.

[39] S. D. Ahmed, F. S. M. Al-Ismail, M. Shafiullah, F. A. Al-Sulaiman, and I. M. El-Amin, "Grid integration challenges of wind energy: A review," *IEEE Access*, vol. 8, pp. 10857–10878, 2020, doi: 10.1109/ACCESS.2020.2964896.

[40] M. Shafiullah, S. D. Ahmed, and F. A. Al-Sulaiman, "Grid integration challenges and solution strategies for solar PV systems: A review," *IEEE Access*, vol. 10, pp. 52233–52257, 2022, doi: 10.1109/ACCESS.2022.3174555.

[41] M. Ali, M. I. Hossain, and M. Shafiullah, "Fuzzy logic for energy management in hybrid energy storage systems integrated DC microgrid," in *Proc. Int. Conf. Power Energy Syst. Appl. (ICoPESA)*, Feb. 2022, pp. 424–429, doi: 10.1109/ICOPESA54515.2022.9754406.

[42] M. I. Hossain, M. Shafiullah, and M. A. Abido, "Battery power control strategy for intermittent renewable energy integrated modular multilevel converter-based high-voltage direct current network," *Sustainability*, vol. 15, no. 3, p. 2626, Feb. 2023, doi: 10.3390/SU15032626.

[43] M. N. Hellesnes, K. Sharifabadi, and S. A. S. S. Acevedo. (2017). *Use of Battery Energy Storage for Power Balancing in a Large-Scale HVDC Connected Wind Power Plant*. NTNU. [Online]. Available: https://ntnuopen.ntnu.no/ntnu-xmlui/handle/11250/2454582

[44] I. P. Reite. (2017). *Battery Energy Storage System Connected to a Three-Phase 50 Hz-Grid*. NTNU. [Online]. Available: https://ntnuopen.ntnu.no/ntnu-xmlui/handle/11250/2453622

[45] Y. Ma, H. Lin, Z. Wang, and Z. Ze, "Modified state-of-charge balancing control of modular multilevel converter with integrated battery energy storage system," *Energies*, vol. 12, no. 1, p. 96, Dec. 2018, doi: 10.3390/en12010096.

[46] G. Wang, G. Konstantinou, C. D. Townsend, J. Pou, S. Vazquez, G. D. Demetriades, and V. G. Agelidis, "A review of power electronics for grid connection of utility-scale battery energy storage systems," *IEEE Trans. Sustain. Energy*, vol. 7, no. 4, pp. 1778–1790, Oct. 2016, doi: 10.1109/TSTE.2016.2586941.

[47] T. Soong and P. W. Lehn, "Evaluation of emerging modular multilevel converters for BESS applications," *IEEE Trans. Power Del.*, vol. 29, no. 5, pp. 2086–2094, Oct. 2014, doi: 10.1109/TPWRD.2014.2341181.

[48] M. Hagiwara and H. Akagi, "Control and experiment of pulsewidth-modulated modular multilevel converters," *IEEE Trans. Power Electron.*, vol. 24, no. 7, pp. 1737–1746, Jul. 2009, doi: 10.1109/TPEL.2009.2014236.

[49] B. Xiao, F. Filho, and L. M. Tolbert, "Single-phase cascaded H-bridge multilevel inverter with nonactive power compensation for grid-connected photovoltaic generators," in *Proc. IEEE Energy Convers. Congr. Expo.*, Sep. 2011, pp. 2733–2737, doi: 10.1109/ECCE.2011.6064135.

[50] Q. Chen, R. Li, and X. Cai, "Analysis and fault control of hybrid modular multilevel converter with integrated battery energy storage system," *IEEE J. Emerg. Sel. Topics Power Electron.*, vol. 5, no. 1, pp. 64–78, Mar. 2017, doi: 10.1109/JESTPE.2016.2623672.

[51] A. Lachichi, "Modular multilevel converters with integrated batteries energy storage," in *Proc. Int. Conf. Renew. Energy Res. Appl. (ICRERA)*, Oct. 2014, pp. 828–832, doi: 10.1109/ICRERA.2014.7016501.

[52] I. Trintis, S. Munk-Nielsen, and R. Teodorescu, "A new modular multilevel converter with integrated energy storage," in *Proc. 37th Annu. Conf. IEEE Ind. Electron. Soc.*, Nov. 2011, pp. 1075–1080, doi: 10.1109/IECON.2011.6119457.

[53] T. Soong. (2015). *Modular Multilevel Converters With Integrated Energy Storage*. [Online]. Available: https://tspace.library.utoronto.ca/handle/1807/71617

[54] F. Nadeem, S. M. S. Hussain, P. K. Tiwari, A. K. Goswami, and T. S. Ustun, "Comparative review of energy storage systems, their roles, and impacts on future power systems," *IEEE Access*, vol. 7, pp. 4555–4585, 2019, doi: 10.1109/ACCESS.2018.2888497.

[55] M. C. Argyrou, P. Christodoulides, and S. A. Kalogirou, "Energy storage for electricity generation and related processes: Technologies appraisal and grid scale applications," *Renew. Sustain. Energy Rev.*, vol. 94, pp. 804–821, Oct. 2018, doi: 10.1016/j.rser.2018.06.044.

[56] M. Swierczynski, R. Teodorescu, C. N. Rasmussen, P. Rodriguez, and H. Vikelgaard, "Overview of the energy storage systems for wind power integration enhancement," in *Proc. IEEE Int. Symp. Ind. Electron.*, Jul. 2010, pp. 3749–3756, doi: 10.1109/ISIE.2010.5638061.

[57] S. R. Salkuti and C. M. Jung, "Comparative analysis of storage techniques for a grid with renewable energy sources," *Int. J. Eng. Technol.*, vol. 7, no. 3, pp. 970–976, Jun. 2018, doi: 10.14419/ijet.v7i3.12728.

[58] M. Ahmed, S. Kuriry, M. D. Shafiullah, and M. A. Abido, "DC microgrid energy management with hybrid energy storage systems," in *Proc. 23rd Int. Conf. Mechatronics Technol. (ICMT)*, Oct. 2019, pp. 1–6, doi: 10.1109/ICMECT.2019.8932147.

[59] P. F. Ribeiro, B. K. Johnson, M. L. Crow, A. Arsoy, and Y. Liu, "Energy storage systems for advanced power applications," *Proc. IEEE*, vol. 89, no. 12, pp. 1744–1756, 2001, doi: 10.1109/5.975900.

[60] Z. Chen, X. Zou, S. Duan, and H. Wei, "Power conditioning system of flywheel energy storage," in *Proc. 8th Int. Conf. Power Electron.*, May 2011, pp. 2763–2768, doi: 10.1109/ICPE.2011.5944769.

[61] M. Amiryar and K. Pullen, "A review of flywheel energy storage system technologies and their applications," *Appl. Sci.*, vol. 7, no. 3, p. 286, Mar. 2017, doi: 10.3390/APP7030286.

[62] F. Diaz-Gonzalez, A. Sumper, O. Gomis-Bellmunt, and R. Villafafila-Robles, "Modeling and validation of a flywheel energy storage lab-setup," in *Proc. 3rd IEEE PES Innov. Smart Grid Technol. Eur.*, Oct. 2012, pp. 1–12, doi: 10.1109/ISGTEUROPE.2012.6465640.

[63] G. Nair S and N. Senroy, "Power smoothening using multi terminal DC based DFIG connection and flywheel energy storage system," in *Proc. IEEE 6th Int. Conf. Power Syst. (ICPS)*, Mar. 2016, pp. 1–6, doi: 10.1109/ICPES.2016.7584134.

[64] R. G. Gadelrab, M. S. Hamad, A. S. Abdel-Khalik, and A. E. Zawawi, "Wind farms-fed HVDC system power profile enhancement using solid state transformer based flywheel energy storage system," *J. Energy Storage*, vol. 4, pp. 145–155, Dec. 2015, doi: 10.1016/j.est.2015.10.003.

[65] M. I. Daoud, A. M. Massoud, A. S. Abdel-Khalik, A. Elserougi, and S. Ahmed, "A flywheel energy storage system for fault ride through support of grid-connected VSC HVDC-based offshore wind farms," *IEEE Trans. Power Syst.*, vol. 31, no. 3, pp. 1671–1680, May 2016, doi: 10.1109/TPWRS.2015.2465163.

[66] K. H. Ahmed, A. S. Abdel-Khalik, A. Elserougi, A. Massoud, and S. Ahmed, "Fault ride-through capability enhancement based on flywheel energy storage system for wind farms connected via VSC high voltage DC transmission," in *Proc. 10th IET Int. Conf. AC DC Power Transmiss. (ACDC)*, 2012, pp. 1–13, doi: 10.1049/cp.2012.1988.

[67] I. A. Gowaid, A. A. Elserougi, A. S. Abdel-Khalik, A. M. Massoud, and S. Ahmed, "A series flywheel architecture for power levelling and mitigation of DC voltage transients in multi-terminal HVDC grids," *IET Gener., Transmiss. Distrib.*, vol. 8, no. 12, pp. 1951–1959, Dec. 2014, doi: 10.1049/iet-gtd.2013.0953.

[68] M. I. Daoud, A. Massoud, S. Ahmed, A. S. Abdel-Khalik, and A. Elserougi, "Ride-through capability enhancement of VSC-HVDC based wind farms using low speed flywheel energy storage system," in *Proc. IEEE Appl. Power Electron. Conf. Expo.*, Mar. 2014, pp. 2706–2712, doi: 10.1109/APEC.2014.6803687.

[69] M. I. Daoud, A. Massoud, A. Elserougi, A. Abdel-Khalik, and S. Ahmed, "A dual three-phase induction machine based flywheel storage system driven by modular multilevel converters for fault ride through in HVDC systems," in *Proc. IEEE PES Asia–Pacific Power Energy Eng. Conf. (APPEEC)*, Nov. 2015, pp. 1–5, doi: 10.1109/APPEEC.2015.7380870.

[70] L. Yang, Z. Xu, J. Ostergaard, Z. Y. Dong, and K. P. Wong, "Advanced control strategy of DFIG wind turbines for power system fault ride through," *IEEE Trans. Power Syst.*, vol. 27, no. 2, pp. 713–722, May 2012, doi: 10.1109/TPWRS.2011.2174387.

[71] X. Zeng, T. Liu, S. Wang, Y. Dong, and Z. Chen, "Comprehensive coordinated control strategy of PMSG-based wind turbine for providing frequency regulation services," *IEEE Access*, vol. 7, pp. 63944–63953, 2019, doi: 10.1109/ACCESS.2019.2915308.

[72] K. S. Tey and S. Mekhilef, "Modified incremental conductance MPPT algorithm to mitigate inaccurate responses under fast-changing solar irradiation level," *Sol. Energy*, vol. 101, pp. 333–342, Mar. 2014, doi: 10.1016/J.SOLENER.2014.01.003.

[73] S. Motahhir, A. El Hammoumi, and A. El Ghzizal, "The most used MPPT algorithms: Review and the suitable low-cost embedded board for each algorithm," *J. Cleaner Prod.*, vol. 246, Feb. 2020, Art. no. 118983, doi: 10.1016/J.JCLEPRO.2019.118983.

[74] A. Yazdani and P. P. Dash, "A control methodology and characterization of dynamics for a photovoltaic (PV) system interfaced with a distribution network," *IEEE Trans. Power Del.*, vol. 24, no. 3, pp. 1538–1551, Jul. 2009, doi: 10.1109/TPWRD.2009.2016632.
[75] A. Yazdani and R. Iravani, *Voltage-Sourced Converters in Power Systems? Modeling, Control, and Applications*. Hoboken, NJ, USA: Wiley, 2010.
[76] K. Sharifabadi, L. Harnefors, H. P. Nee, S. Norrga, and R. Teodorescu, *Design, Control and Application of Modular Multilevel Converters for HVDC Transmission Systems*. Hoboken, NJ, USA: Wiley, 2016.
[77] F. Martinez-Rodrigo, D. Ramirez, A. B. Rey-Boue, S. De Pablo, and L. C. Herrero-De Lucas, "Modular multilevel converters: Control and applications," *Energies*, vol. 10, no. 11, pp. 1–10, 2017.
[78] M. I. Hossain, M. Shafiullah, and M. Abido, "VSC controllers for multiterminal HVDC transmission system: A comparative study," *Arabian J. Sci. Eng.*, vol. 45, no. 8, pp. 6411–6422, Aug. 2020, doi: 10.1007/s13369-020-04500-y.
[79] A. Soomro, M. E. Amiryar, K. R. Pullen, and D. Nankoo, "Comparison of performance and controlling schemes of synchronous and induction machines used in flywheel energy storage systems," *Energy Proc.*, vol. 151, pp. 100–110, Oct. 2018, doi: 10.1016/J.EGYPRO.2018.09.034.
[80] J. Van Mierlo, "Models of energy sources for EV and HEV: Fuel cells, batteries, ultracapacitors, flywheels and engine-generators," *J. Power Sources*, vol. 128, no. 1, pp. 76–89, Mar. 2004, doi: 10.1016/J.JPOWSOUR.2003.09.048.

MD ISMAIL HOSSAIN received the B.Sc. degree in electrical and electronics engineering from RUET, Bangladesh, in 2009, the M.Sc. degree in electrical and electronics engineering from BUET, Bangladesh, in 2013, and the Ph.D. degree in electrical engineering from the King Fahd University of Petroleum and Minerals (KFUPM), Saudi Arabia, in 2021. He is currently a Postdoctoral Researcher with the Interdisciplinary Research Center for Renewable Energy and Power Systems (IRC-REPS), KFUPM. Before joining the Ph.D. program, he was an Assistant Professor with the Electrical and Electronics Engineering Department, IIUC, Bangladesh. His research interests include renewable energy and battery-based voltage and frequency regulation, inertia emulation, ac/dc microgrid design and control, grid compliance converter, power electronics, multiterminal HVDC transmission networks, motor drives, and renewable energy integration.

WALEED M. HAMANAH received the B.Sc. degree in electrical engineering from Sana'a University, Yemen, in June 2008, and the M.Sc. and Ph.D. degrees in electrical engineering from the King Fahd University of Petroleum and Minerals (KFUPM), Dhahran, Saudi Arabia, in 2016 and 2021, respectively. From September 2008 to December 2011, he was an Instructor with Taiz University, Yemen. He is currently a Postdoctoral Researcher with the Interdisciplinary Research Center of Renewable Energy and Power Systems (IRC-REPS), Research Institute, KFUPM. His research interests include renewable energy, power electronics, machines, control, and saving energy.

MD SHAFIUL ALAM received the B.Sc. degree in electrical and electronic engineering (EEE) from the Dhaka University of Engineering and Technology, Gazipur, Bangladesh, the M.Sc. degree in EEE from the Bangladesh University of Engineering and Technology, Dhaka, Bangladesh, and the Ph.D. degree in electrical engineering from the King Fahd University of Petroleum and Minerals (KFUPM), Saudi Arabia. He started his career as a Faculty Member with the Department of EEE, International Islamic University Chittagong (IIUC), Bangladesh, in August 2008, where his highest rank was Associate Professor. He was a Postdoctoral Fellow with the K. A. CARE Energy Research and Innovation Center (ERIC), KFUPM, from March 2020 to March 2022. He is currently a Research Engineer III with the Applied Research Center for Environment and Marine Studies (ARCEMS), Research Institute, KFUPM. He worked on several funded projects during Ph.D. research. His research interests include energy and environment, greenhouse gas emission management, data analysis, renewable energy sources integration into the utility grid, ac/dc microgrids, high-voltage dc transmission, voltage source converter control, fault current limiter, optimization algorithms, fuzzy logic, neural networks, and machine learning. He is a member of the Institution of Engineers Bangladesh. He was a recipient of best paper awards at many IEEE international conferences.

MD SHAFIULLAH (Senior Member, IEEE) received the B.Sc. and M.Sc. degrees in electrical and electronic engineering (EEE) from the Bangladesh University of Engineering and Technology (BUET), Bangladesh, in 2009 and 2013, respectively, and the Ph.D. degree in electrical power and energy systems from the King Fahd University of Petroleum and Minerals (KFUPM), Saudi Arabia, in 2018. He was a Faculty Member with the Department of Electrical and Electronic Engineering, International Islamic University of Chittagong (IIUC), Bangladesh, from 2009 to 2013. He is currently an Assistant Professor (Research Engineer III) with the Interdisciplinary Research Center for Renewable Energy and Power Systems (IRC-REPS), KFUPM. His research interests include grid fault diagnosis, grid integration of renewable energy resources, power quality analysis, power system control and stability, evolutionary algorithms, and machine learning techniques.

MOHAMMAD A. ABIDO (Senior Member, IEEE) received the B.Sc. (Hons.) and M.Sc. degrees in EE from Menoufia University, Shebin El-Kom, Egypt, in 1985 and 1989, respectively, and the Ph.D. degree from the King Fahd University of Petroleum and Minerals (KFUPM), Dhahran, Saudi Arabia, in 1997. He is currently a Distinguished University Professor with KFUPM, and also a Senior Researcher with the K. A. CARE (ERIC), Dhahran. He participated in more than 50 funded projects and supervised more than 50 M.S. and Ph.D. students. He has published two books and more than 350 research articles. His research interests include power system stability, planning, and optimization techniques applied to power systems. He was a recipient of the KFUPM Excellence in Research Award, in 2002, 2007, and 2012, the KFUPM Best Project Award, in 2007 and 2010, the First Prize Paper Award of the Industrial Automation and Control Committee of the IEEE Industry Applications Society, in 2003, the Abdel-Hamid Shoman Prize for Young Arab Researchers in Engineering Sciences, in 2005, the Best Applied Research Award of the 15th GCC-CIGRE Conference, Abu Dhabi, United Arab Emirates, in 2006, and the Best Poster Award from the International Conference on Renewable Energies and Power Quality (ICREPQ 2013), Bilbao, Spain, in 2013. He received the Almarai Prize for Scientific Innovation, Distinguished Scientist, Saudi Arabia, in 2018, and the Khalifa Award for Education, Higher Education, Distinguished University Professor in Scientific Research, Abu Dhabi, in 2018.